

Sum Rate Maximization in the Constant Envelope MIMO Downlink with the RZF Precoder

Ferhad Askerbeyli, *Graduate Student Member, IEEE*, Wen Xu, *Senior Member, IEEE*, Josef A. Nossek, *Life Fellow, IEEE*

Abstract—Feeding power amplifiers (PAs) with constant envelope (CE) signals is an effective way to reduce the power consumption in massive multiple input multiple output (MIMO) systems. The nonlinear distortion caused by CE signaling must be mitigated by means of signal processing to improve the achievable sum rates. To this purpose, many linear and nonlinear precoding techniques have been developed for the CE MIMO downlink. The vast majority of these CE precoding techniques do not include a power allocation scheme, which is indispensable to achieve adequate performances in the downlink with channel gain imbalances between users. In this paper, we present two algorithms to produce a power allocation scheme for regularized zero-forcing (RZF) precoding in CE MIMO downlink. Both techniques are based on transforming the CE quantized MIMO downlink to an approximately equivalent system of parallel single-input-single-output (SISO) channels. The first technique is proven to solve the sum rate maximization problem in the approximate system optimally, whereas the second technique obtains the local maximum with lower complexity. We also extend another state-of-the-art quantization aware sum rate maximization algorithm with linear precoding to the CE downlink. Numerical results illustrate significant gains for the performance of the RZF precoder when the CE quantization is taken into account in a power allocation. Another key numerical result is that the proposed RZF techniques achieve almost the identical performance so that the one with lower computational complexity is chosen as the main method. Results also show that the proposed RZF precoding schemes perform at least as good as the state-of-the-art method with an advantage that the main RZF method has significantly lower computational complexity than the state-of-the-art.

Index Terms—MIMO downlink, RZF precoder, CE transmit signals, power allocation, asymptotic analysis, sum rate maximization

I. INTRODUCTION

For 5G and beyond mobile communications, massive multiple input multiple output (MIMO) is a key technology to achieve target performances in spectral efficiency, reliability and coverage [1]–[3]. Implementation of a fully digital massive MIMO requires a radio frequency (RF) chain for each antenna element separately. As a result, fully digital massive MIMO system suffers from a low energy efficiency due to high number of active RF chain components such as

digital-to-analog converters (DACs), analog-to-digital converters (ADCs), power amplifiers (PAs), mixers etc.

One approach to recover the energy efficiency is to reduce power consumption of the RF chain components, especially the components that contribute to the power consumption most. In the downlink, which is the scenario of our interest in this study, the primary way to recover energy efficiency is to maximize the PA efficiency, since PA is the most power-hungry component in the RF chain on the transmitter side [4]. For linear PAs, the drain efficiency is maximized by ensuring that PA input signals have a fixed magnitude in all channel uses, i.e., by feeding PAs with constant envelope (CE) signals [5]. Furthermore, CE signals enable use of nonlinear PAs, which are designed to operate at very high power efficiency. The secondary way is to reduce the power consumption of DACs by decreasing their resolution. Employing 1-bit DACs serves both primary and secondary ways, as it minimizes the power consumption at the digital-to-analog conversion while generating CE input signals.

CE signaling and use of low resolution DACs come at a cost of severe quantization distortion that significantly deteriorates the transmit signal. Thus, many linear and nonlinear precoding techniques have been developed to suppress the quantization distortion and achieve target performances in the quantized systems with high energy efficiency. Symbol-wise nonlinear precoding methods especially have been successful in achieving solid data and error rates by suppressing the quantization distortion for every transmission individually [6]–[8].

The above-mentioned quantized precoding techniques are designed for the downlink where users have a common large-scale fading coefficient and they fail in channels with varying large-scale fading coefficients for different users. In this case, a power allocation mechanism prioritizing between users is indispensable to achieve the satisfactory sum or error rate performances. An arising challenge in quantized systems is to develop a precoding technique that simultaneously handles the power allocation and the quantization distortion.

A. Related Works

Power allocation for the MIMO downlink with high resolution DACs has been studied extensively. For instance, power allocation for the weighted sum rate maximization in high resolution downlink with zero-forcing (ZF) precoding is a convex problem and it is solved by the well-known water-filling algorithm [9]. A broader class of linear precoding is defined by regularized zero-forcing (RZF), where the channel inversion operation is controlled via a regularization parameter.

This paper was presented in part at 2023 *IEEE 98th Vehicular Technology Conference (VTC2023-Fall)*.

F. Askerbeyli is with School of Computation, Information and Technology, Technical University of Munich (TUM), 80333 Munich, Germany and also with Munich Research Center, Huawei Technologies Duesseldorf GmbH, 80992 Munich, Germany (e-mail: ferhad.askerbeyli@tum.de).

J. A. Nossek is with School of Computation, Information and Technology, Technical University of Munich (TUM), 80333 Munich, Germany (e-mail: josef.a.nossek@tum.de).

W. Xu is with Munich Research Center, Huawei Technologies Duesseldorf GmbH, 80992 Munich, Germany (wen.xu@ieee.org).

Weighted sum rate maximization with the RZF precoding is a problem of finding the optimal regularization parameter and the power allocation jointly and unlike with the ZF precoding, the problem is not convex. Furthermore, analysis of the exact system is very difficult compared to the ZF case. In [10], a broad analysis of the MIMO downlink with RZF precoding is provided by utilizing the large system approximation. A power allocation scheme for MIMO downlink with RZF is also included in [10]. However, the power allocation in [10] is not for users with different large-scale fading coefficients, but for users with different quality of channel state information at the transmitter (CSIT). Authors of [11] derived joint optimality conditions for power allocation, user loading and regularization to maximize the sum rate in MIMO downlink with the RZF precoding. Unlike [10], power allocation in [11] is to tackle the channel gain imbalances between users. In [12], power allocation that minimizes the transmit power while satisfying individual signal-to-interference and noise ratio (SINR) constraints is obtained and examined via the large system approximation.

Studies on quantized systems with ZF or RZF precoding have also been reported. Authors of [13] combined the large system approximation with the Busgang decomposition to provide a performance analysis of MIMO downlink with ZF precoding and 1-bit DACs. A similar analysis for the MIMO downlink with ZF precoder and CE quantization is done in [14], where the error rate performance is improved by introducing a Gaussian dither to the precoded signal. Analysis of MIMO downlink with 1-bit DACs and RZF precoding is done in [15] to optimize the regularization parameter and the user loading.

None of [10]–[15] considered power allocation and quantization together. The first study with power allocation mechanism and quantization awareness is [16], where energy efficiency maximization problem of the MIMO downlink with low-resolution DACs is solved by optimizing all elements of a linear precoding matrix jointly. A special case of energy efficiency optimization problem in [16] is the sum rate maximization, which implicitly includes a power allocation problem as well. In contrast to [16], a quantization aware power allocation scheme, which aims at sum rate maximization in the 1-bit MIMO downlink with ZF precoding, is explicitly formulated with a power factor per each user in [17].

B. Main Contributions

Employing RZF precoders with power allocation in [11] and [12] for CE quantized systems is clearly suboptimal, as they disregard the quantization distortion. Previously in [18], we handled this suboptimality by proposing 1-bit quantization aware power allocation for RZF precoding. In this paper, we extend the heuristic method in [18] to the CE downlink with higher resolution and provide a novel method that solves the same problem as the heuristic method optimally. Contributions of this work are summarized as follows:

- An asymptotic analysis of a MIMO downlink with RZF precoding and CE transmit signals is provided by combining the large system approximation with high transmit power assumption. The asymptotic analysis leads to

derivation of an approximately equivalent system with parallel single-input-single-output (SISO) channels.

- Two algorithms that obtain a power allocation and a regularization parameter to maximize the sum rate in the approximate system are proposed. One of the algorithms with branch and bound method obtains the global maximum for the approximate system. The other algorithm with alternating optimization converges to a local maximum.
- Behavior of the alternating algorithm at high transmit power regime and its computational complexity are analyzed in detail.
- The state-of-the-art quantization aware linear precoding method in [16] is nontrivially extended for the CE quantization case. Later it is used for comparison with the proposed RZF precoding techniques.

The asymptotic analysis and the alternating algorithm are presented in [18], the other contributions (including the analysis of the alternating algorithm) are introduced for the first time.

Two most relevant works to ours are [11] and [15], where the former excludes the CE quantization and the latter excludes the power allocation. Both [11] and [15] mainly focus on user-loading problem and the latter considers only 1-bit quantization. This work considers a system in the intersection of the settings in [11] and [15], i.e., it is a nontrivial generalization of both regarding the power allocation problem.

On the contrary to the quantization aware generalized power iterations for spectral efficiency maximization (Q-GPI-SEM) algorithm from [16], we impose the RZF structure on the linear precoding matrix. By doing so, we reduce the joint optimization of the whole precoding matrix to the joint optimization of power factors of users, regularization parameter and number of users to serve, which reduces the computational complexity. Furthermore, the methods we propose are compatible with any input constellation, whereas Q-GPI-SEM's performance deteriorates if the input signal is not Gaussian.

C. Remainder and Notation

The structure of this paper is as follows: System model is introduced in Section II. The approximate signal-to-quantization, interference and noise ratios (SQINRs) of users are computed in Section III by utilizing the asymptotic analysis. An approximately equivalent system of parallel SISO channels based on the approximate SQINRs is presented in Section IV. Two algorithms that perform sum rate maximization for this approximate system are devised in Section V. A high transmit power and complexity analysis of the alternating algorithm is presented in Section VI. The Q-GPI-SEM algorithm is extended to CE quantized systems in Section VII. Numerical results and conclusions are reported in Section VIII and Section IX, respectively.

Notation: The m th entry of vector \mathbf{a} and the (m, n) th entry of matrix \mathbf{A} are denoted as a_m or $[\mathbf{a}]_m$ and $a_{m,n}$ or $[\mathbf{A}]_{m,n}$, respectively. Expressions $\text{diag}(\mathbf{A})$, $\text{diag}(\mathbf{a})$ and $\text{diag}(a_1, a_2, \dots, a_n)$ stand for diagonal matrices with the entries of the diagonal of matrix \mathbf{A} , vector \mathbf{a} and vector $[a_1, a_2, \dots, a_n]$, respectively. The covariance matrix between vectors \mathbf{a} and \mathbf{b} is denoted as $\mathbf{C}_{\mathbf{ab}}$. A circularly symmetric

complex Gaussian distribution with the mean \mathbf{m} and covariance \mathbf{C} is denoted as $\mathcal{CN}(\mathbf{m}, \mathbf{C})$. The term $\text{vec}(\mathbf{A})$ denotes the vector obtained by stacking columns of \mathbf{A} . The closed interval between a and b is denoted as $[a, b]$.

II. SYSTEM MODEL AND PROBLEM FORMULATION

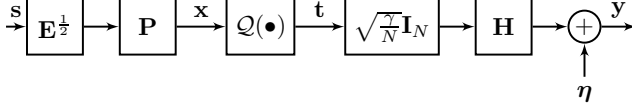


Fig. 1. MIMO downlink with linear precoding and CE quantization.

Fig. 1 illustrates the MIMO downlink of our interest, which consists of a transmitter with N antennas and M single-antenna users with $M \leq N$. The channel between the transmitter and single-antenna users is modeled as $\mathbf{H} = \mathbf{\Sigma}^{\frac{1}{2}} \tilde{\mathbf{H}} \in \mathbb{C}^{M \times N}$, where $\mathbf{\Sigma} = \text{diag}(\sigma_1, \dots, \sigma_M)$ contains the large-scale fading coefficients of all users in nonincreasing order such that $\sigma_1 \geq \sigma_2 \geq \dots \geq \sigma_M$ and matrix $\tilde{\mathbf{H}} \in \mathbb{C}^{M \times N}$ consists of uncorrelated elements with $[\tilde{\mathbf{H}}]_{m,n} \sim \mathcal{CN}(0, 1) \forall m, n$. We denote the m th row of \mathbf{H} and $\tilde{\mathbf{H}}$ as \mathbf{h}_m^H and $\tilde{\mathbf{h}}_m^H$, respectively and $\mathbf{h}_m^H = \sqrt{\sigma_m} \tilde{\mathbf{h}}_m^H$.

The input signal $\mathbf{s} \in \mathbb{C}^M$ consists of zero mean, independent and identically distributed (i.i.d.) symbols with unit variance, i.e., $\mathbb{E}[\mathbf{s}] = \mathbf{0}$ and $\mathbb{E}[\mathbf{s}\mathbf{s}^H] = \mathbf{I}$, that are to be transmitted to the corresponding user. There is no restriction other than all input symbols have a common constellation and distribution.

A two-stage linear precoding scheme is employed. In the first stage, the input signal \mathbf{s} is weighted by $\mathbf{E}^{\frac{1}{2}}$, where $\mathbf{E} = \text{diag}(e_1, e_2, \dots, e_M)$ is the power allocation matrix and $e_m \geq 0$ is the power factor of the m th user. In the second stage, mapping of \mathbf{s} to the precoded signal \mathbf{x} is carried out as $\mathbf{x} = \mathbf{P}\mathbf{E}^{\frac{1}{2}}\mathbf{s}$, where \mathbf{P} is the precoding matrix determined according to the CSIT. Power factors in \mathbf{E} set the received signal powers at users and should be tuned carefully to achieve high sum rates especially in channels with various large-scale fading coefficients for different users. As some users may have very weak channels, it may be optimal to allocate power only to a subset of users with the strongest channels such that $e_1, e_2, \dots, e_K > 0$ and $e_{K+1} = e_{K+2} = \dots = e_M = 0$. In such cases, symbols of users with indices from $K+1$ to M do not contribute to the precoded signal, i.e., they do not get served.

For the second stage, we consider the RZF precoding which reads as follows when all M users are taken into account

$$\mathbf{P} = (\tilde{\mathbf{H}}^H \tilde{\mathbf{H}} + \alpha \mathbf{I}_N)^{-1} \tilde{\mathbf{H}}^H \mathbf{\Sigma}^{-\frac{1}{2}}. \quad (1)$$

Equation (1) is a controlled inversion of the small-scale fading matrix $\tilde{\mathbf{H}}$ with a nonnegative regularization parameter α and inversion of the large-scale fading matrix $\mathbf{\Sigma}^{\frac{1}{2}}$. As power allocation may cause only a subset of users to get served, the RZF precoding does not always need to take all users into account. For that reason, we define the RZF precoder depending on the maximum number of users we aim to serve. The RZF precoding we employ for K users reads as

$$\mathbf{P} = [\mathbf{P}_K \quad \mathbf{0}] = \left[(\tilde{\mathbf{H}}_K^H \tilde{\mathbf{H}}_K + \alpha \mathbf{I}_N)^{-1} \tilde{\mathbf{H}}_K^H \mathbf{\Sigma}_K^{-\frac{1}{2}} \quad \mathbf{0} \right], \quad (2)$$

where $\tilde{\mathbf{H}}_K \in \mathbb{C}^{K \times N}$ consists of first K rows of $\tilde{\mathbf{H}}$ and $\mathbf{\Sigma}_K = \text{diag}(\sigma_1, \sigma_2, \dots, \sigma_K)$. The RZF in (2) leads to the following precoding

$$\mathbf{x} = \mathbf{P}_K \mathbf{E}_K^{\frac{1}{2}} \mathbf{s}_K = \sum_{k=1}^K \sqrt{e_k} \mathbf{p}_k s_k, \quad (3)$$

where $\mathbf{E}_K = \text{diag}(e_1, e_2, \dots, e_K)$ and $\mathbf{s}_K = [s_1 s_2 \dots s_K]^T$ and \mathbf{p}_k is the k th column of \mathbf{P}_K . As a result, design of the two-stage RZF precoder consists of jointly determining number of users to serve, power allocation for the served users and the regularization parameter. Note that RZF precoding in (2) includes (1) as a special case of $K = M$.

Elements of the precoded signal $\mathbf{x} \in \mathbb{C}^N$ go through the following CE quantization with Q levels

$$t_n = \mathcal{Q}(x_n) = \exp(j(\lceil \frac{\angle x_n}{2\psi} \rceil - \psi)), \forall n, \quad (4)$$

where $\psi = \frac{\pi}{Q}$, i.e., every precoded symbol is mapped to one of the Q discrete points with unit magnitude. We also use the vector notation for this element-wise quantization as $\mathbf{t} = \mathcal{Q}(\mathbf{x})$. Note that the power of quantized signal \mathbf{t} is equal to N and CE quantization is invariant to scaling of \mathbf{x} with a positive constant v such that $\mathcal{Q}(x) = \mathcal{Q}(vx)$. At PAs, the quantized signal \mathbf{t} is scaled by factor of $\sqrt{\frac{\gamma}{N}}$ to produce a transmit signal with power of γ . The transmit signal \mathbf{t} propagates through channel \mathbf{H} and is received at single-antenna users with additive white Gaussian noise (AWGN) of $\boldsymbol{\eta} \sim \mathcal{CN}(\mathbf{0}_M, \mathbf{I}_M)$ as follows

$$\mathbf{y} = \sqrt{\frac{\gamma}{N}} \mathbf{H} \mathbf{t} + \boldsymbol{\eta}. \quad (5)$$

In this paper, our primary goal is to obtain a two-stage RZF precoding scheme that maximizes the sum rate of the CE quantized downlink described in Fig. 1. Since two-stage RZF precoding can be parametrized by K , \mathbf{E}_K and α , the sum rate maximization problem can be formulated as follows

$$\max_{\substack{\alpha \geq 0, K \in \{1, 2, \dots, M\} \\ e_1, e_2, \dots, e_K \geq 0}} \sum_{k=1}^K I(y_k; s_k), \quad (6)$$

where $I(y_k; s_k)$ is the mutual information between the k th input and received signal.

Solving (6) directly is challenging, since derivation of an analytic expression for the rate of the k th user $I(y_k; s_k)$ is difficult as the distribution of \mathbf{s} is arbitrary and CE quantization takes place. We instead approximately compute SQINR values of the system and then identify an equivalent system of parallel SISO channels with the help of computed SQINRs. In the end, the sum rate maximizing algorithm is developed based on the approximately equivalent system of parallel SISO channels.

III. COMPUTATION OF SQINR

In this section, we compute SQINRs of the system described in Section II, when RZF precoding is done for K users. To this aim, we need to decompose the received signal at the k th user into uncorrelated components and compute the powers of these components.

A. Received Signal Decomposition

A linear relationship between s_k and y_k is not immediately available because of the CE quantization. Bussgang decomposition is conventionally applied to formulate the CE

quantization in (4) as a linear stochastic process to circumvent the nonlinearity as follows [6], [13]

$$\mathbf{t} = \mathbf{B}\mathbf{x} + \mathbf{d} = \mathbf{B}\mathbf{P}_K \mathbf{E}_K^{\frac{1}{2}} \mathbf{s}_K + \mathbf{d}, \quad (7)$$

where \mathbf{B} is the Bussgang gain matrix and \mathbf{d} is the distortion vector [19]. Bussgang gain matrix \mathbf{B} for CE quantization of \mathbf{x} with Q levels as $\mathbf{t} = \mathcal{Q}(\mathbf{x})$ is computed in [20] as

$$\mathbf{B} = \xi_Q \text{diag}(\mathbf{C}_{\mathbf{x}\mathbf{x}})^{-\frac{1}{2}}, \quad (8)$$

with

$$\xi_Q = \frac{Q}{2\sqrt{\pi}} \sin\left(\frac{\pi}{Q}\right). \quad (9)$$

Note that ξ_Q solely depends on the number of quantization levels Q and it increases as Q increases and $\lim_{Q \rightarrow \infty} \xi_Q = \sqrt{\frac{\pi}{4}}$. For our case, the key property of Bussgang decomposition is that if \mathbf{x} is Gaussian distributed, then \mathbf{t} is decomposed into two uncorrelated components \mathbf{d} and $\mathbf{B}\mathbf{x}$. The decomposition in (7) can still be used if \mathbf{x} is not Gaussian, however, in this case \mathbf{d} would not be uncorrelated with \mathbf{x} . Note that \mathbf{d} is certainly not Gaussian so that assuming Gaussian \mathbf{d} at the receivers would lead to mismatched decoding.

By combining (8), (7), (5) and (3), one can write the received signal for the k th user as

$$y_k = \sqrt{\frac{\gamma}{N}} e_k \xi_Q \mathbf{h}_k^H \text{diag}(\mathbf{C}_{\mathbf{x}\mathbf{x}})^{-\frac{1}{2}} \mathbf{p}_k s_k + \sqrt{\frac{\gamma}{N}} \mathbf{h}_k^H \mathbf{d} + \sqrt{\frac{\gamma}{N}} \xi_Q \mathbf{h}_k^H \text{diag}(\mathbf{C}_{\mathbf{x}\mathbf{x}})^{-\frac{1}{2}} \sum_{j \neq k} \sqrt{e_j} \mathbf{p}_j s_j + \eta_k, \quad (10)$$

for $k = 1, 2, \dots, K$. In (10), the received signal is decomposed as the component that is linearly dependent on input s_k , the received quantization distortion, the multi-user interference (MUI) and the additive noise, respectively. Yet, computing the exact SQINR of the k th user is still very difficult by (10) since the quantization distortion vector \mathbf{d} is not uncorrelated from the input signal \mathbf{s} , unless \mathbf{x} is Gaussian. Furthermore, computing the exact power of the linearly dependent component, MUI and quantization distortion in terms of regularization parameter α is very difficult. For those reasons, we resort to asymptotic approximation.

B. Asymptotic Approximation

The difficulty we encounter in computing the exact SQINR values of the system described in Fig. 1 is present in [11] and [15], where researchers resorted to asymptotic approximation, as we also follow here.

Asymptotic approximation is typically used interchangeably with the so-called "large system approximation", which consists of approximating metrics of a MIMO system under the assumption that $M \rightarrow \infty, N \rightarrow \infty$ with a fixed user load $\beta = \frac{M}{N}$. Large system approximation is based on one of the key merits of massive MIMO known as channel hardening. As dimensions of a MIMO system get large, the system effectively acts more deterministic, i.e., SINR/SQINR at the receivers do not depend on the channel realization \mathbf{H} , but they depend on the channel dimensions M, N . For any system with a finite M, N and a given β , an approximate system based on the large system approximation can be obtained and used to develop algorithms for the original system.

In our scenario, we assume a more realistic channel model including large-scale fading coefficients and thus power factor

matrix \mathbf{E}_K is also involved in precoding. For that reason, the typical large system approximation is not sufficient to characterize the overall system in (10). To overcome this problem, we additionally assume that number of users K for which RZF precoding is designed is large and

$$\mathbf{E}_K \boldsymbol{\Sigma}_K^{-1} \approx \frac{\text{tr}(\mathbf{E}_K \boldsymbol{\Sigma}_K^{-1})}{K} \mathbf{I}_K. \quad (11)$$

In Section VI-A, we show that these assumptions get more accurate at the high transmit power regime for the algorithms we present. Thus, we refer to these two additional assumptions together as the high transmit power assumption. Note that (11) is not imposed as a constraint when optimizing \mathbf{E}_K , but it serves to only identify an approximate system which get more accurate at high transmit power regime.

1) Large System Approximation

Let us first recap few identities from random matrix theory that we repeatedly use for large system approximation.

Lemma 1. (Corollary 1 in [21]) Let \mathbf{A} be a deterministic $N \times N$ complex matrix with bounded spectral radius for all N . Let $\tilde{\mathbf{h}}_k \in \mathbb{C}^{N \times 1}$ consist of i.i.d complex random variables with zero mean, unit variance and finite eight moment. Then, $\frac{1}{N} \tilde{\mathbf{h}}_k^H \mathbf{A} \tilde{\mathbf{h}}_k \approx \frac{1}{N} \text{tr}(\mathbf{A})$. (12)

Theorem 1. (Theorem 7 in [21]) For $\tilde{\mathbf{H}}_K \in \mathbb{C}^{K \times N}$ consisting of i.i.d elements $[\tilde{\mathbf{H}}_K]_{m,n} \sim \mathcal{CN}(0, 1)$, when $K \rightarrow \infty, N \rightarrow \infty$ with fixed ratio $\beta = \frac{K}{N}$, it holds that

$$\text{tr}((\tilde{\mathbf{H}}_K^H \tilde{\mathbf{H}}_K + \alpha \mathbf{I}_N)^{-1}) \approx g(\beta, \rho), \quad (13)$$

where $g(\beta, \rho)$ satisfies

$$g(\beta, \rho) = \left(\rho + \frac{\beta}{1 + g(\beta, \rho)} \right)^{-1} \quad (14)$$

with the normalized regularization parameter $\rho = \frac{\alpha}{N}$. Notice that $g(\beta, \rho)$ is positive by definition, since it is an asymptotic value of trace of a positive semidefinite matrix. The positive solution of (14) is given as

$$g(\beta, \rho) = \frac{\sqrt{(\beta + \rho - 1)^2 + 4\rho} - (\beta + \rho - 1)}{2\rho}. \quad (15)$$

For the rest of this paper, let us introduce $\mathbf{M}_K = (\tilde{\mathbf{H}}_K^H \tilde{\mathbf{H}}_K + \alpha \mathbf{I}_N)^{-1}$ to ease the notation.

Corollary 1. ([11]) The following approximation holds under the same conditions as Theorem 1

$$-\alpha \text{tr}(\mathbf{M}_K^2) \approx \rho \frac{\partial g(\beta, \rho)}{\partial \rho}. \quad (16)$$

Corollary 1 can be easily derived by taking the derivative of (13) with respect to α on both sides.

By applying simple algebraic manipulations on (14), we can obtain the following identities

$$\beta + \rho(1 + g(\beta, \rho))^2 = \frac{(1 + g(\beta, \rho))^2 - \beta g^2(\beta, \rho)}{g(\beta, \rho)} \quad (17)$$

and

$$\frac{\partial g(\beta, \rho)}{\partial \rho} = -\frac{g(\beta, \rho)(1 + g(\beta, \rho))^2}{\beta + \rho(1 + g(\beta, \rho))^2}. \quad (18)$$

For a given β , equation (18) implies that $g(\beta, \rho)$ is strictly decreasing in ρ , since $g(\beta, \rho) > 0$ and $\rho \geq 0$. Furthermore, one can show that

$$\lim_{\rho \rightarrow \infty} g(\beta, \rho) = 0 \quad (19)$$

with a simple manipulation of (15).

2) An Alternative Regularization Parameter

Let us introduce the following term

$$u(\beta, \rho) = \frac{g(\beta, \rho)}{1 + g(\beta, \rho)}, \quad (20)$$

for which it is implied that $\lim_{\rho \rightarrow \infty} u(\beta, \rho) = 0$ due to (19). By manipulating (14) and (15), we compute that $\lim_{\rho \rightarrow 0} u(\beta, \rho) = 1$ for $\beta \leq 1$. The derivative of (20) yields

$$\frac{\partial u(\beta, \rho)}{\partial \rho} = \frac{1}{(1 + g(\beta, \rho))^2} \frac{\partial g(\beta, \rho)}{\partial \rho}, \quad (21)$$

which implies that $u(\beta, \rho)$ is strictly decreasing in ρ , since from (18) we inferred that $\frac{\partial g(\beta, \rho)}{\partial \rho} < 0$. Hence, for a fixed value of β , $u(\beta, \rho)$ starts as 1 at $\rho = 0$ and strictly decreases to 0 as $\rho \rightarrow \infty$. We hence can use u as an alternative regularization parameter with a one-to-one relationship to α

$$\alpha(u) = N \left(\frac{1}{u} - \beta \right) (1 - u), \quad (22)$$

which is obtained by combining (14), (20) and definition of $\rho = \frac{\alpha}{N}$. Note that we denoted $u(\beta, \rho)$ as u for the sake of brevity, as we do for the rest of this paper. From (22), we observe that as RZF precoder approaches to ZF precoder u approaches to 1 and as RZF precoder approaches to maximum ratio transmission (MRT) precoder, u approaches to 0.

In the rest of the current section, the approximate power of the desired signal component and MUI is expressed in terms of u . On the contrary to the other regularization parameter ρ , which is accompanied by $g(\beta, \rho)$ in signal or MUI power expressions (see [11], [15]), u solely reflects the effect of regularization on the approximate power of the desired signal component and MUI. This makes use of u more practical as it leads to more intuitive and compact expressions.

C. Application of Asymptotic Approximation

By combining $\text{diag}(\mathbf{C}_{\text{xx}}) = \text{diag}(\mathbf{P}_K \mathbf{E}_K \mathbf{P}_K^H)$ and $\mathbf{P}_K = \mathbf{M}_K \tilde{\mathbf{H}}_K^H \Sigma_K^{-\frac{1}{2}}$, we apply the asymptotic approximation to $\text{diag}(\mathbf{C}_{\text{xx}})$ as follows

$$\begin{aligned} \text{diag}(\mathbf{C}_{\text{xx}}) &= \text{diag}(\mathbf{M}_K \tilde{\mathbf{H}}_K^H \mathbf{E}_K \Sigma_K^{-1} \tilde{\mathbf{H}}_K \mathbf{M}_K) \\ &\stackrel{(a)}{\approx} \frac{\text{tr}(\mathbf{E}_K \Sigma_K^{-1})}{K} \text{diag}(\mathbf{M}_K \tilde{\mathbf{H}}_K^H \tilde{\mathbf{H}}_K \mathbf{M}_K) \\ &\stackrel{(b)}{=} \frac{\text{tr}(\mathbf{E}_K \Sigma_K^{-1})}{K} \text{diag}(\mathbf{M}_K - \alpha \mathbf{M}_K^2) \\ &\stackrel{(c)}{\approx} \frac{\text{tr}(\mathbf{E}_K \Sigma_K^{-1})}{K} \left(\frac{\text{tr}(\mathbf{M}_K)}{N} - \alpha \frac{\text{tr}(\mathbf{M}_K^2)}{N} \right) \mathbf{I}_N. \end{aligned} \quad (23)$$

Step (a) is taken by employing (11), step (b) is taken by employing $\tilde{\mathbf{H}}_K^H \tilde{\mathbf{H}}_K \mathbf{M}_K = \mathbf{I}_N - \alpha \mathbf{M}_K$, step (c) is by approximating $\text{diag}(\mathbf{M}_K) \approx \frac{\text{tr}(\mathbf{M}_K)}{N} \mathbf{I}_N$, when K is large.

We proceed on approximating $\text{diag}(\mathbf{C}_{\text{xx}})$ by replacing (13) and (16) in (23) and then making use of (17) and (18)

$$\begin{aligned} \text{diag}(\mathbf{C}_{\text{xx}}) &\approx \frac{\text{tr}(\mathbf{E}_K \Sigma_K^{-1})}{KN} (g(\beta, \rho) + \rho \frac{\partial g(\beta, \rho)}{\partial \rho}) \mathbf{I}_N \\ &= \frac{\text{tr}(\mathbf{E}_K \Sigma_K^{-1})}{KN} \frac{\beta u^2}{(1 - \beta u^2)} \mathbf{I}_N. \end{aligned} \quad (24)$$

1) Power of the Desired Signal

By combining (24) and $\mathbf{p}_k = \frac{1}{\sqrt{\sigma_k}} \mathbf{M}_K \tilde{\mathbf{h}}_k$, desired signal at the k th user in (10) is approximated as

$$y_k^{(s)} \approx \sqrt{\frac{\gamma w_k \sigma_k (1 - \beta u^2)}{\beta u^2}} \xi_Q \tilde{\mathbf{h}}_k^H \mathbf{M}_K \tilde{\mathbf{h}}_k s_k, \quad (25)$$

where we also introduced

$$w_k = \frac{e_k / \sigma_k}{\text{tr}(\mathbf{E}_K \Sigma_K^{-1})} K \geq 0 \text{ for } k = 1, 2, \dots, K. \quad (26)$$

The following approximation can be derived by following the same steps as in Appendix A of [11], where matrix inversion lemma has been utilized

$$|\tilde{\mathbf{h}}_k^H \mathbf{M}_K \tilde{\mathbf{h}}_k|^2 \approx \frac{g^2(\beta, \rho)}{(1 + g(\beta, \rho))^2} = u^2. \quad (27)$$

As a result, the signal power can be approximated as

$$P_k^{(s)} \approx \xi_Q^2 \gamma \sigma_k w_k \left(\frac{1}{\beta} - u^2 \right), \quad (28)$$

In (28), increasing u leads to decrease in signal power.

2) Power of the MUI

Let us now approximate the MUI signal as follows

$$\begin{aligned} y_k^{(\text{mui})} &= \sqrt{\frac{\gamma}{N}} \xi_Q \mathbf{h}_k^H \text{diag}(\mathbf{C}_{\text{xx}})^{-\frac{1}{2}} \sum_{j \neq k} \sqrt{\frac{e_j}{\sigma_j}} \mathbf{M}_K \tilde{\mathbf{h}}_j s_j \\ &\approx \sqrt{\frac{\gamma}{N} \frac{\sigma_k}{\text{tr}(\mathbf{E}_K \Sigma_K^{-1}) \frac{\beta u^2}{1 - \beta u^2}}} \xi_Q \sum_{j \neq k} \sqrt{\frac{e_j}{\sigma_j}} \tilde{\mathbf{h}}_k^H \mathbf{M}_K \tilde{\mathbf{h}}_j s_j. \end{aligned} \quad (29)$$

Power of the MUI is then approximated as

$$P_k^{(\text{mui})} \approx \xi_Q^2 \frac{\gamma}{N} \frac{\sigma_k}{\text{tr}(\mathbf{E}_K \Sigma_K^{-1}) \frac{\beta u^2}{1 - \beta u^2}} \sum_{j \neq k} \frac{e_j}{\sigma_j} |\tilde{\mathbf{h}}_k^H \mathbf{M}_K \tilde{\mathbf{h}}_j|^2 \quad (30)$$

In [11], the term $|\tilde{\mathbf{h}}_k^H \mathbf{M}_K \tilde{\mathbf{h}}_j|^2$ is approximated as

$$|\tilde{\mathbf{h}}_k^H \mathbf{M}_K \tilde{\mathbf{h}}_j|^2 \approx \frac{1}{N} \frac{g(\beta, \rho)}{(1 + g(\beta, \rho))^2 (\beta + \rho(1 + g(\beta, \rho))^2)}. \quad (31)$$

By plugging in (31) and (17) to (30), the MUI power can be written as

$$P_k^{(\text{mui})} \approx \xi_Q^2 \gamma \sigma_k (1 - u)^2 \frac{1}{K} \sum_{j \neq k} w_j \quad (32)$$

By employing the definition of w_k in (26) and the high transmit power assumption in (11), we can write

$$\frac{1}{K} \sum_{j \neq k} w_j \approx 1 - \frac{1}{K}. \quad (33)$$

Eventually, power of the MUI at the k th user reads as

$$P_k^{(\text{mui})} \approx \xi_Q^2 \gamma \sigma_k \frac{K-1}{K} (1 - u)^2. \quad (34)$$

In (34), increase in u leads to decrease in MUI power.

3) Power of the Received Quantization Distortion

Power of the quantization distortion at the k th user in (10) is given as

$$P_k^{(q)} = \frac{\gamma}{N} \mathbf{h}_k^H \mathbf{C}_{\text{dd}} \mathbf{h}_k = \frac{\gamma \sigma_k}{N} \tilde{\mathbf{h}}_k^H \mathbf{C}_{\text{dd}} \tilde{\mathbf{h}}_k, \quad (35)$$

where \mathbf{C}_{dd} is the covariance matrix of the quantization distortion \mathbf{d} . Except the case of 1-bit quantization i.e., CE quantization with $Q = 4$, it is difficult to compute \mathbf{C}_{dd} exactly.

For that reason, we again resort to the asymptotic analysis. Lemma 1 in (12) implies that

$$\frac{1}{N} \tilde{\mathbf{h}}_k^H \mathbf{C}_{dd} \tilde{\mathbf{h}}_k \approx \frac{1}{N} \text{tr}(\mathbf{C}_{dd}), \quad (36)$$

which leads to the following approximation

$$P_k^{(q)} \approx \frac{\gamma \sigma_k}{N} \text{tr}(\mathbf{C}_{dd}). \quad (37)$$

Recall that asymptotic approximation assumptions include K being large so that the precoded signal $\mathbf{x} = \mathbf{P}_K \mathbf{E}_K^{\frac{1}{2}} \mathbf{s}_K$ can be approximated Gaussian due to central limit theorem (CLT) [22]. By using Bussgang decomposition in (7) and the fact that $\mathbb{E}[\mathbf{x} \mathbf{d}^H] \approx \mathbf{0}$ with approximately Gaussian \mathbf{x} , we write the following approximation

$$\begin{aligned} \text{tr}(\mathbf{C}_{tt}) &= \text{tr}(\mathbb{E}[(\mathbf{B}\mathbf{x} + \mathbf{d})(\mathbf{B}\mathbf{x} + \mathbf{d})^H]) \\ &\approx \xi_Q^2 \text{tr}(\text{diag}(\mathbf{C}_{xx})^{-\frac{1}{2}} \mathbf{C}_{xx} \text{diag}(\mathbf{C}_{xx})^{-\frac{1}{2}}) + \text{tr}(\mathbf{C}_{dd}). \end{aligned} \quad (38)$$

Diagonals of \mathbf{C}_{tt} and $\text{diag}(\mathbf{C}_{xx})^{-\frac{1}{2}} \mathbf{C}_{xx} \text{diag}(\mathbf{C}_{xx})^{-\frac{1}{2}}$ consist of ones. As a result, power of the distortion \mathbf{d} reads as

$$\text{tr}(\mathbf{C}_{dd}) \approx (1 - \xi_Q^2)N. \quad (39)$$

Eventually, quantization distortion power is computed as

$$P_k^{(q)} \approx (1 - \xi_Q^2) \gamma \sigma_k \quad (40)$$

4) Approximate SQINR

At this step, we again resort to the asymptotic analysis assumption that K is large, which helps us to characterize the precoded signal \mathbf{x} as approximately Gaussian due to CLT. In this case, the quantization distortion \mathbf{d} and \mathbf{s} can be considered uncorrelated so that we can combine (28), (34) and (40) to approximate the SQINR at the k th user as follows

$$\text{SQINR}_k(w_k, u) \approx \frac{(\frac{1}{\beta} - u^2)}{\tau(1-u)^2 + c_k} w_k, \text{ for } k = 1, 2 \dots K, \quad (41)$$

where we introduced and $\tau = \frac{K-1}{K}$ and

$$c_k = \frac{1}{\xi_Q^2} \left(1 + \frac{1}{\gamma \sigma_k}\right) - 1. \quad (42)$$

An important fact that we use later is $c_k > 0$, since for CE quantized systems $\xi_Q < 1$. Furthermore, the approximate SQINR in (41) is not changed with positive scaling of \mathbf{E}_K since positive scaling of \mathbf{E}_K does not change (w_1, w_2, \dots, w_K) in (26). This is due to CE quantization being invariant to scaling with a positive term such that $\mathcal{Q}(\mathbf{x}) = \mathcal{Q}(v\mathbf{x})$.

Equation (41) can be used to approximate the systems with infinite resolution quantization by setting ξ_Q to 1. Such an approximation is equivalent to approximation of SINR in [11]. Yet, due to especially making use of (17) and introduction of u , (41) is more compact than its counterpart [11, Eq. (4)]. Also, equation (41) is more intuitive as it shows how regularization affects powers of the desired signal and MUI, whereas such an observation cannot be made in [11, Eq. (4)].

IV. APPROXIMATELY EQUIVALENT SYSTEM

Equation (41) shows the approximate SQINRs, when RZF precoder is designed for K users. The exact achievable rates of users cannot be computed via (41), since distribution of the quantization distortion \mathbf{d} is not available in an analytic form. Instead, a lower bound to the achievable rates of the system in (41) is defined by assuming a mismatched decoder at the receiver [23]. We here consider that receivers decode based on

the Gaussian auxiliary channel, i.e., the decoding is done by assuming the quantization distortion is Gaussian distributed. This system with mismatched decoding is equivalent to the following system of K parallel SISO channels

$$y_k = \sqrt{\lambda_k(u)} w_k s_k + \eta_k, \quad (43a)$$

$$\lambda_k(u) = \frac{(\frac{1}{\beta} - u^2)}{\tau(1-u)^2 + c_k}, \quad (43b)$$

$$w_k = \frac{K \frac{e_k}{\sigma_k}}{\text{tr}(\mathbf{E}_K \boldsymbol{\Sigma}_K^{-1})} \text{ for } k = 1, 2, \dots, K, \quad (43c)$$

where s_k and η_k are the same input and the noise signals as in (10), and $\lambda_k(u)$ and w_k are the channel gain and the transmit power of the k th user, respectively. Note that (43c) imposes a transmit power constraint $\sum_{k=1}^K w_k = K$ and the receive signal-to-noise ratio (SNR) of the k th user reads as $\text{SNR}_k(u, w_k) = \lambda_k(u) w_k$, which is equal to approximate SQINR in (41). Furthermore, the channel gains are in nonincreasing order such that $\lambda_1(u) \geq \lambda_2(u) \dots \geq \lambda_K(u)$, because of large-scale fading coefficients being in nonincreasing order. For the sake of brevity, we introduce the transmit power vector $\mathbf{w} = [w_1, w_2, \dots, w_K]^T$.

The K parallel SISO channels system in (43) is approximately equivalent to the quantized MIMO downlink system in (10). There is a one-to-one relation between the original and the alternative regularization parameters α and u , which is given by (22). A relation between \mathbf{w} and \mathbf{E}_K , which is helpful to transform one into the other, is also present in (43c). As a result, sum rate maximization of system in Fig. 1 can approximately be done via the parallel SISO channels system in (43). To this aim, we formulate and solve the sum rate maximization problem for system in (43).

A. Sum Rate Maximization of the Approximate System

The original sum rate maximization problem (6) can be transformed to sum rate maximization for (43) as follows

$$\begin{aligned} \underset{\substack{u \in [0,1], \\ K \in \{1,2,\dots,M\}, \\ \mathbf{w} \geq \mathbf{0}_K}}{\text{argmax}} \quad & \sum_{k=1}^K I(\lambda_k(u, K) w_k) \text{ s.t. } \sum_{k=1}^K w_k = K, \end{aligned} \quad (44)$$

where $I(\lambda_k(u, K) w_k) = I(s_k; \sqrt{\lambda_k(u, K)} w_k s_k + \eta_k)$ is the mutual information between the input signal s_k and received signal y_k . Notice that we changed the notation from $\lambda_k(u)$ to $\lambda_k(u, K)$ since we now consider K also as an optimization variable. Essentially, we now see the channel gain $\lambda_k(u, K)$ dependent on K via $\beta(K) = \frac{K}{N}$ and $\tau(K) = \frac{K-1}{K}$.

A well-known result from [24] states that the mutual information between the k th input and output $I_k(\lambda_k(u, K) w_k)$ is a concave function of $\lambda_k(u, K) w_k$. However, as $\lambda_k(u, K)$ is not concave in u , the objective function of (44) is not jointly concave in \mathbf{w} , u and K . Typically a nonconvex optimization with $M+2$ variables such as (44) is impractical due to its high computational complexity even for moderate values of M . Yet, as we use the alternative regularization parameter u in formulating (44) and the optimal power allocation for fixed (u, K) can be computed, we can provide a method that obtains the global maximum with an feasible computational complexity. Let us first discuss the power allocation problem

with fixed u and K , which provides a basis for the algorithms we devise to solve (44).

B. Power Allocation with Fixed u and K

For a parallel SISO system with fixed u and K , the sum rate maximization is reduced to the following convex problem

$$\mathbf{w}^*(u, K) = \underset{\mathbf{w} \geq \mathbf{0}}{\operatorname{argmax}} \sum_{k=1}^K I_k(\lambda_k(u, K)w_k) \text{ s.t. } \sum_{k=1}^K w_k = K. \quad (45)$$

The optimal solution of problem (45) is given in [25] as

$$w_k^*(u, K) = \frac{1}{\lambda_k(u, K)} \operatorname{MMSE}^{-1}(\min(1, \frac{\mu}{\lambda_k(u, K)})) \forall k, \quad (46)$$

with μ satisfying

$$\sum_{\substack{k=1, \\ \lambda_k(u, K) > \mu}}^K \frac{1}{\lambda_k(u, K)} \operatorname{MMSE}^{-1}(\frac{\mu}{\lambda_k(u, K)}) = K. \quad (47)$$

The function $\operatorname{MMSE}^{-1}(\bullet)$, with the domain in the interval $[0, 1]$, is the inverse function of $\operatorname{MMSE}(\operatorname{SNR})$, which is the minimum mean square error achieved by the conditional mean estimator in the channel

$$y_k = \sqrt{\operatorname{SNR}s_k} + \eta_k, \quad (48)$$

where $\eta_k \sim \mathcal{CN}(0, 1)$ and s_k has the same distribution as in (43a). The value of $\operatorname{MMSE}(\operatorname{SNR})$ can be computed offline by integration over the complex field and it depends on the distribution of s_k . For the details on computing $\operatorname{MMSE}(\operatorname{SNR})$, the reader is referred to [25]. A look-up table can then be generated to implement the function $\operatorname{MMSE}^{-1}(\bullet)$ by using the pre-computed values of $\operatorname{MMSE}(\bullet)$. The value of μ satisfying (47) can be found by the bisection search method and using the generated look-up table. This procedure of obtaining solutions for (46) and (47) is referred as mercury/waterfilling [25].

V. SUM RATE MAXIMIZATION ALGORITHMS

We here present the branch and bound method and the alternating optimization to solve (44). The former has significantly higher computational complexity than the latter, yet it obtains the global maximum, whereas the latter algorithm converges to a local maximum.

A. Global Optimization via the Branch and Bound Method

As the sum rate maximizing power allocation vector for fixed u and K is given as $\mathbf{w}^*(u, K)$, problem (44) can be rewritten as

$$\max_{(u, K) \in \mathcal{S}_0} \sum_{k=1}^K I(\lambda_k(u, K)w_k^*(u, K)), \quad (49)$$

with $\mathcal{S}_0 = \{(u, K) | u \in [0, 1], K \in \{1, 2, \dots, M\}\}$ such that the optimization variables are reduced to u and K .

To solve (49), we modify the mixed monotonic programming (MMP) framework from [26], which enables an efficient application of the branch and bound algorithm [27, Sec. 6.2]. The branch and bound method consists of a search for the global optimum by systematically dividing an initial constraint set into disjoint subsets and checking which subsets potentially contain the optimum via defined upper and lower bounds. In our case, the initial set which contains the global maximum is given as \mathcal{S}_0 ,

For a given subset $\mathcal{S} = \{(u, K) | u \in [u_L, u_U], K \in \{K_L, \dots, K_U\}\}$, the maximum sum rate can be formulated as

$$R(\mathcal{S}) = \max_{(u, K) \in \mathcal{S}} \max_{\mathbf{w} \geq \mathbf{0}} \sum_{k=1}^K I(\lambda_k(u, K)w_k) \text{ for } \sum_{k=1}^K w_k = K. \quad (50)$$

An upper bound to (50) can be defined as

$$U(\mathcal{S}) = \max_{\mathbf{w} \geq \mathbf{0}} \sum_{k=1}^{K_U} I(A_k(u_L, u_U, K_L)w_k) \text{ s.t. } \sum_{k=1}^{K_U} w_k = K_U, \quad (51)$$

where we introduce the enhanced channel gain for the k th user as

$$A_k(u_L, u_U, K_L) = \frac{(\frac{1}{\beta(K_L)} - u_L^2)}{\tau(K_L)(1 - u_U)^2 + c_k} \quad (52)$$

for $k = 1, \dots, K_U$. When introducing $A_k(u_L, u_U, K_L)$, we apply the mixed monotonic (MM) formulation to $\lambda_k(u, K)$ such that we replace u in the numerator and denominator of (43b) by u_L and u_U , respectively and K by K_L . As the numerator and denominator in (43b) are decreasing in u and $\lambda_k(u, K)$ is decreasing in K , it holds that

$$A_k(u_L, u_U, K_L) \geq \max_{(u, K) \in \mathcal{S}} \lambda_k(u, K) \text{ for } k = 1, \dots, K_U. \quad (53)$$

To see the whole derivation of upper bound (51), the reader is referred to Appendix A.

A lower bound to $R(\mathcal{S})$ can be generated by using any element $(u, K) \in \mathcal{S}$ and the corresponding optimal $\mathbf{w}^*(u, K)$. Here, we select (u_U, K_L) to generate the lower bound as follows

$$L(\mathcal{S}) = \sum_{k=1}^{K_L} I(\lambda_k(u_U, K_L)w_k^*(u_U, K_L)). \quad (54)$$

With the upper and lower bounds defined in (51) and (54), we apply two tests on a subset to see if it potentially contains the solution of (49). The first one is to check if a subset's upper bound is smaller than a lower bound of any other subset. Such a subset is guaranteed not to contain the solution of (49) and it can be discarded from the search. The second test is to check if the optimal power allocation vector in (51), which we denote as $\mathbf{w}_U(\mathcal{S})$, has less nonzero entries than K_L . In Appendix B, Theorem 4 states that such subsets do not contain the solution of (49).

Note that generating the upper and lower bounds with given $A_k(u_L, u_U, K_L)$, $\mathbf{w}_U(\mathcal{S})$, $\lambda_k(u_U, K_L)$, $w_k^*(u_U, K_L)$ requires to compute mutual information $I(\operatorname{SNR})$ for a given SNR value. This can be again implemented by offline numerical integration and use of the look-up tables.

Application of the branch and bound method to solve (49) is described in Algorithm 1. First, the set \mathbb{S} , which is the union of all disjoint subsets that potentially contain the maximizer of (49), is initialized as $\mathbb{S} = \{\mathcal{S}_0\}$. Then, the upper bounds to the sum rates of all disjoint subsets in \mathbb{S} are computed. All subsets that have $\mathbf{w}_U(\mathcal{S})$ with less nonzero elements than K_L are removed from further search at Step 3. Then, the lower bounds to the maximum sum rates for the remaining subsets in \mathbb{S} are computed. Subsets with a smaller upper bound than the maximum lower bound of all subsets are removed from \mathbb{S} at Step 5. At Step 6, the subset with the highest upper bound $\hat{\mathcal{S}} = \{(u, K) | u \in [\hat{u}_L, \hat{u}_U], K \in \{\hat{K}_L, \dots, \hat{K}_U\}\}$ is replaced

Algorithm 1 Branch and Bound for (49)

- 1: Initialize union set all subsets as $\mathbb{S} = \{\mathcal{S}_0\}$.
 - 2: Compute $U(\mathcal{S})$ for each subset in \mathbb{S} by (51).
 - 3: Check $w_U(\mathcal{S})$ for each subset in \mathbb{S} . Remove every subset with $w_U(\mathcal{S})$ containing less nonzero elements than its \hat{K}_L .
 - 4: Compute $L(\mathcal{S})$ for each subset in \mathbb{S} by (54)
 - 5: Remove subsets with $U(\mathcal{S}) < \max_{\mathcal{S} \in \mathbb{S}} L(\mathcal{S})$.
 - 6: Find the subset $\hat{\mathcal{S}} = \operatorname{argmax}_{\mathcal{S} \in \mathbb{S}} U(\mathcal{S})$. Replace \mathbb{S} by $\{\mathbb{S} \setminus \hat{\mathcal{S}}\} \cup \{\mathcal{S}_1, \mathcal{S}_2\}$ by using (55) and (56).
 - 7: Repeat Steps 2-6 until $\max_{\mathcal{S} \in \mathbb{S}} U(\mathcal{S}) - \max_{\mathcal{S} \in \mathbb{S}} L(\mathcal{S}) \leq \epsilon$
 - 8: Return u_U, K_L and $\mathbf{w}^*(u_U, K_L)$ of subset $\operatorname{argmax}_{\mathcal{S} \in \mathbb{S}} L(\mathcal{S})$
-

by two disjoint subsets \mathcal{S}_1 and \mathcal{S}_2 which are determined in two following ways. If $\hat{u}_U - \hat{u}_L > \hat{K}_U - \hat{K}_L$, then it is set

$$\begin{aligned} \mathcal{S}_1 &= \{(u, K) | u \in [\hat{u}_L, \frac{\hat{u}_L + \hat{u}_U}{2}], K \in \{\hat{K}_L, \dots, \hat{K}_U\}\} \\ \mathcal{S}_2 &= \{(u, K) | u \in [\frac{\hat{u}_L + \hat{u}_U}{2}, \hat{u}_U], K \in \{\hat{K}_L, \dots, \hat{K}_U\}\} \end{aligned} \quad (55)$$

else if $\hat{u}_U - \hat{u}_L \leq \hat{K}_U - \hat{K}_L$, it is set

$$\begin{aligned} \mathcal{S}_1 &= \{(u, K) | u \in [\hat{u}_L, \hat{u}_U], K \in \{\hat{K}_L, \dots, \lfloor \frac{\hat{K}_L + \hat{K}_U}{2} \rfloor\}\} \\ \mathcal{S}_2 &= \{(u, K) | u \in [\hat{u}_L, \hat{u}_U], K \in \{\lfloor \frac{\hat{K}_L + \hat{K}_U}{2} \rfloor + 1, \dots, K_U\}\}. \end{aligned} \quad (56)$$

Upper bounds of \mathcal{S}_1 and \mathcal{S}_2 are refined such that they are certainly less than or equal to the upper bound of $\hat{\mathcal{S}}$. As a result, repeating steps between 2 and 6 eliminates the subsets that are guaranteed not to contain the maximizer of (49) and the remaining subsets are divided into smaller subsets so that the gap between the remaining upper and lower bounds decrease. As the initial set \mathcal{S}_0 contains the global maximum, the convergence proof in [26] suggests that it is guaranteed obtain ϵ -optimal solution for (49) with Algorithm 1. Note that the MM formulation in (52), which enables solving (49) optimally, is not possible without introduction of u .

B. Suboptimal Sum Rate Maximization via Alternating Optimization

The second algorithm we propose to solve (44) is an alternating optimization process where \mathbf{w} is updated by solving (45) for a fixed (u, K) and u is updated by solving the sum rate maximization for fixed \mathbf{w} and K . To this aim, we formulate the problem of finding the optimal u with fixed K and \mathbf{w} as

$$u^*(\mathbf{w}, K) = \operatorname{argmax}_{u \in [0,1]} \sum_{k=1}^K I(\lambda_k(u, K) w_k). \quad (57)$$

As $\lambda_k(u, K)$ is not concave in u , (57) is not a convex problem. Yet, we can obtain a local maximum for (57) by solving

$$\sum_{k=1}^K \frac{\partial I(\operatorname{SNR}_k(u, w_k))}{\partial u} \Big|_{u=u^*(\mathbf{w}, K)} = 0. \quad (58)$$

We switched notation to $\operatorname{SNR}_k(u, w_k) = \lambda_k(u, K) w_k$, for the sake of brevity. To obtain u^* , we first use the chain rule

$$\frac{\partial I(\operatorname{SNR}_k(w_k, u))}{\partial u} = \frac{\partial I(\operatorname{SNR}_k(w_k, u))}{\partial \operatorname{SNR}_k(w_k, u)} \frac{\partial \operatorname{SNR}_k(w_k, u)}{\partial u}. \quad (59)$$

For the first term on the right in (59), we know that [24]

$$\frac{\partial I(\operatorname{SNR}_k(w_k, u))}{\partial \operatorname{SNR}_k(w_k, u)} = \frac{\operatorname{MMSE}(\operatorname{SNR}_k(w_k, u))}{\ln 2}. \quad (60)$$

The second term on the right hand side of (59) reads as

$$\frac{\partial \operatorname{SNR}_k(w_k, u)}{\partial u} = \frac{-2c_k u + 2\tau(1-u)(\frac{1}{\beta} - u)}{(\tau(1-u)^2 + c_k)^2} w_k. \quad (61)$$

By using (61) and (60), we execute a bisection search to find a local maximum in $[0, 1]$. We use the MMSE look-up table generated to compute the mercury/waterfilling solution of (47) to compute (59). Theorem 2 implies a local maximum of (57) is certainly obtained by bisection search for (58).

Theorem 2. There exists at least one u value that satisfies (58) in interval $[0, 1]$.

Proof. In this proof, we denote $u^*(\mathbf{w}, K)$ as u^* for the sake of brevity. First, let us consider the case with $K = 1$, where we compute that

$$\frac{\partial \operatorname{SNR}_1(w_1, u)}{\partial u} = -2 \frac{u}{c_1} w_1. \quad (62)$$

For $K = 1$, it holds that

$$\frac{\partial I(\operatorname{SNR}_1(w_1, u))}{\partial u} \Big|_{u=u^*} = -2 \frac{\operatorname{MMSE}(\operatorname{SNR}_1(w_1, u^*))}{\ln 2} \frac{u^* w_1}{c_1}, \quad (63)$$

which is equal to 0 only if $u^* = 0$, since c_1 and $\operatorname{MMSE}(\operatorname{SNR}_1(w_1, u^*))$ are strictly positive. Hence, a local maximum in $[0, 1]$ is obtained at $u^* = 0$.

Now let us consider $K \geq 2$. Observe that the denominator in (61) is positive and w_k is nonnegative. Hence, the sign of (61) is simply determined by the sign of the convex quadratic expression $-2c_k u + 2\tau(1-u)(\frac{1}{\beta} - u)$. We compute that

$$(-2c_k u + 2\tau(1-u)(\frac{1}{\beta} - u)) \Big|_{u=0} = 2\frac{\tau}{\beta} > 0, \quad (64)$$

which implies $\sum_{k=1}^K \frac{\partial I(\operatorname{SNR}_k(w_k, u))}{\partial u} \Big|_{u=0} > 0$. For $u = 1$, it holds that

$$(-2c_k u + 2\tau(1-u)(\frac{1}{\beta} - u)) \Big|_{u=1} = -2c_k < 0, \quad (65)$$

which implies that $\sum_{k=1}^K \frac{\partial I(\operatorname{SNR}_k(w_k, u))}{\partial u} \Big|_{u=1} < 0$. Thus, there exists a sign change from plus to minus implying the existence of at least one local maximum of the sum rate in $u \in [0, 1]$. \square

Algorithm 2 describes the alternating optimization we propose to solve (44). The algorithm is initialized with the ZF precoder designed for all M users within the coverage area, i.e., $u^{(0)} = 1$ and $K^{(0)} = M$. After the initialization, updates of \mathbf{w} , K and u take place in order until a while loop convergences. A single iteration of the while loop starts with the update of power allocation vector \mathbf{w} at Step 4 according to the most recent channel gains of active users, which are computed in Step 3 as $(\lambda_1, \lambda_2, \dots, \lambda_{K^{(i)}})$. At Step 5, the update of K is done by checking if $\mathbf{w}^{(i+1)}$ has zeros. If there are no zeros, the update is as $K^{(i+1)} = K^{(i)}$. On the other hand, if $\mathbf{w}^{(i+1)}$ has zeros, then designing the RZF precoder with $K^{(i)}$ users is suboptimal. Lemma 3 in Appendix B implies that, higher sum rate is achieved by removing zeros from $\mathbf{w}^{(i+1)}$, setting $K^{(i+1)}$ as the new length of $\mathbf{w}^{(i+1)}$ and scaling $\mathbf{w}^{(i+1)}$. At Step 6, $u^{(i+1)}$ is updated by solving (57)

for fixed $K^{(i+1)}$ and $\mathbf{w}^{(i+1)}$. The process between Steps 3-7 is repeated until convergence for which we select the criteria as $|u^{(i+1)} - u^{(i)}| < \epsilon$.

Algorithm 2 Alternating Optimization to Solve (44)

- 1: Initialize $i = 0$, $u^{(0)} = 1$, $K^{(0)} = M$, $\beta^{(0)} = \frac{K^{(0)}}{N}$, $\tau^{(0)} = \frac{K^{(0)}-1}{K^{(0)}}$.
 - 2: **while** (termination criteria is not met)
 - 3: Compute $(\lambda_1, \lambda_2, \dots, \lambda_{K^{(i)}})$ with $u^{(i)}$, $K^{(i)}$, $\beta^{(i)}$, $\tau^{(i)}$ by using (43b).
 - 4: Solve (45) with computed $(\lambda_1, \lambda_2, \dots, \lambda_{K^{(i)}})$ by the mercury/waterfilling to obtain $\mathbf{w}^{(i+1)}$
 - 5: Check $\mathbf{w}^{(i+1)}$ and remove if there are any zeros. Update $K^{(i+1)}$ as number of elements of $\mathbf{w}^{(i+1)}$. Update $\beta^{(i+1)} = \frac{K^{(i+1)}}{N}$, $\tau^{(i+1)} = \frac{K^{(i+1)}-1}{K^{(i+1)}}$. Update $\mathbf{w}^{(i+1)} = \frac{K^{(i+1)}}{K^{(i)}} \mathbf{w}^{(i)}$.
 - 6: Solve (57) with fixed $\mathbf{w}^{(i+1)}$, $K^{(i+1)}$ to obtain $u^{(i+1)}$.
 - 7: Update $i = i + 1$
 - 8: **end**
 - 9: Return $u^{(i)}$, $K^{(i)}$ and $\mathbf{w}^{(i)}$
-

C. Mapping Back to the Original Parameters

Let us denote the optimized parameters returned by Algorithm 1 and Algorithm 2 as u^* , \mathbf{w}^* and K^* . The obtained (u^*, \mathbf{w}^*) must be mapped back to original parameters (α, \mathbf{E}_K) to precode \mathbf{x} in the actual system in Fig. 1. The regularization parameter is mapped back as $\alpha^* = N(\frac{1}{u^*} - \beta(K^*))(1 - u^*)$ by using the one-to-one relation in (22). On the other hand, the relation between \mathbf{w} and \mathbf{E}_K is not one-to-one and any positive scaling of matrix $\text{diag}(\mathbf{w}^*) \Sigma_{K^*}$ can be used as \mathbf{E}_K , we simply select $\mathbf{E}_K = \text{diag}(\mathbf{w}^*) \Sigma_{K^*}$. Eventually, the RZF precoder is formed as $\mathbf{P}_K = \mathbf{H}_{K^*}^H (\mathbf{H}_{K^*} \mathbf{H}_{K^*}^H + \alpha \Sigma_{K^*})^{-1} \in \mathbb{C}^{N \times K^*}$ and precoding is done as $\mathbf{x} = \mathbf{P}_K \mathbf{E}_K^* \frac{1}{2} \mathbf{s}_{K^*}$.

VI. ANALYSIS OF ALGORITHM 2

A rigorous analysis for overall computational complexity of Algorithm 1 is very difficult, since the number of iterations it requires for convergence depends heavily on the channel realization (especially Step 5). Yet, we empirically recognize that its computational complexity is significantly higher than Algorithm 2. On the other hand, although Algorithm 2 obtains a local maximum for (44), numerical results in Section VIII-A demonstrate that its performance is practically identical to Algorithm 1, which is proven to obtain the global maximum. We thus select Algorithm 2 as the main method to solve (44), whereas Algorithm 1 serves as the benchmark assuring that (44) is solved optimally. Accordingly, we provide the high transmit power and computational complexity analysis only for Algorithm 2.

A. High Transmit Power Regime Analysis

When Algorithm 2 is initialized at high transmit power regime $\gamma \rightarrow \infty$ with $K^{(0)} = M$, the channel gains of the approximate system in (43b) are computed as $\lambda_1(u) \approx \lambda_2(u) \approx \lambda_M(u) = \lambda(u)$, since $c_1 \approx c_2 \approx \dots \approx c_M \approx c = \frac{1}{\xi_Q} - 1$. In this case, the power allocation at Step 4 yields as $\mathbf{w} \approx \mathbf{1}_M$ in

every iteration. Due to (43c), this outcome implies that (11) holds with $K = M$. In conclusion, the assumption that (11) holds and K is large, on which the approximate parallel SISO system in (43) is based on, is accurate for systems with large M at $\gamma \rightarrow \infty$, when Algorithm 2 is employed. This is why we refer to it as high transmit power assumption. Also for Algorithm 1, which is the other algorithm that is based on the assumption that (11) holds and K is large, it is observed that every power allocation vector $\mathbf{w}^*(u_U, K_L)$ that is computed as a candidate for the global maximizer is approximately uniform when $\gamma \rightarrow \infty$. Hence, the high transmit power assumption is valid also for Algorithm 1 at $\gamma \rightarrow \infty$. Note that due to Step 3 of Algorithm 1 and Step 5 of Algorithm 2, the resulting \mathbf{w}^* is not allowed to contain zeros, which improves the accuracy of the assumption in (11).

The following theorem identifies the relationship between total number of users M and the obtained regularization parameter u , when $\gamma \rightarrow \infty$.

Theorem 3. Consider two separate CE quantized systems where a transmitter with N antennas serves M_1 and M_2 users at $\gamma \rightarrow \infty$. Assume $N \geq M_2 > M_1 \geq 2$. For u_1 and u_2 , which are values of u obtained by Algorithm 2 for systems with M_1 and M_2 antennas, respectively, it holds that $u_1 > u_2$.

Proof. Previously in this subsection, it is shown that the power allocation vector is computed as $\mathbf{w} = \mathbf{1}_M$, when Algorithm 2 is employed at $\gamma \rightarrow \infty$. The problem of obtaining optimal u at Step 6 via solving (57) with the fixed $\mathbf{w} = \mathbf{1}_M$ boils down to problem of maximizing common SNR of all users, i.e., to the following problem

$$u^* = \underset{u \in [0,1]}{\text{argmax}} \frac{\frac{1}{\beta(M)} - u^2}{\tau(M)(1-u)^2 + c}. \quad (66)$$

Recall that $\beta(M) = \frac{M}{N}$ and $\tau(M) = \frac{M-1}{M}$. Note that we can compute $\frac{\partial \text{SNR}(u, M)}{\partial u}$ as a specific version of (61) with $w_k = 1$ and $c_k = c > 0$. As it is shown in Section V-B, the sign of the convex quadratic expression $-2cu + 2\tau(M)(1-u)(\frac{1}{\beta(M)} - u)$ is simply the sign of $\frac{\partial \text{SNR}(u, M)}{\partial u}$. Equation (65) shows that there are two roots for $\frac{\partial \text{SNR}(u, M)}{\partial u}$ and $u = 1$ is located between these roots. Furthermore, equation (64) guarantees that the root smaller than 1 is located in interval $[0, 1]$ and it is the only maximizer in $[0, 1]$. Here, we can conclude that there exists a single local maximizer in $[0, 1]$. For a system with given M_1 , let us denote the maximizer as u_1 .

The derivative of $\frac{\partial \text{SNR}(u, M)}{\partial u}$ w.r.t. M leads to

$$\frac{\partial^2 \text{SNR}(u, M)}{\partial u \partial M} = \frac{\partial \left(\frac{-2cu + 2\tau(M)(1-u)(\frac{1}{\beta(M)} - u)}{(\tau(M)(1-u)^2 + c)^2} \right)}{\partial M} < 0. \quad (67)$$

Inequality (67) can be confirmed by inspecting that the numerator is decreasing and the denominator is increasing in M ¹. As a result, it is implied that $\frac{\partial \text{SNR}(u, M)}{\partial u}$ is strictly decreasing in M . We can write that

$$\left. \frac{\partial \text{SNR}(u, M_2)}{\partial u} \right|_{u=u_1} < \left. \frac{\partial \text{SNR}(u, M_1)}{\partial u} \right|_{u=u_1} = 0 \quad (68)$$

¹In the denominator the only quantity that depends on M is $\tau(M) = \frac{M-1}{M}$, which is increasing in M . The derivative of the numerator with respect to M reads as $2(1-u)\frac{N}{M^3}(2-M) - \frac{u}{M^2}$ which negative for $M \geq 2$

for $M_2 > M_1$. We already know that for the system with of M_2 , there exists the maximizer u_2 in $[0, 1]$ for which we can form the following inequality

$$\left. \frac{\partial \text{SNR}(u, M_2)}{\partial u} \right|_{u=u_1} < \left. \frac{\partial \text{SNR}(u, M_2)}{\partial u} \right|_{u=u_2} = 0. \quad (69)$$

Since u_2 is the only root of $\frac{\partial \text{SNR}(u, M_2)}{\partial u}$ in interval $[0, 1]$ and the sign change at $u = u_2$ is from plus to minus, it holds that $u_1 > u_2$. This concludes the proof of Theorem 3. \square

Theorem 3 suggests that at high transmit power regime, ZF precoding becomes more optimal as number of users M decreases down to 2. We can extend Theorem 3 to the infinite resolution scenario, where $c = 0$. In this case, $u = 1$ is the left root of the convex quadratic expression $2\tau(M)(1 - u)(\frac{1}{\beta(M)} - u)$ that determines the sign of $\frac{\partial \text{SNR}(u, M)}{\partial u}$ (The other root satisfies $\frac{1}{\beta}$ is greater than 1, since $\beta \leq 1$). Thus, in infinite resolution systems with $\beta \leq 1$ the maximum in interval $[0, 1]$ is obtained at $u = 1$, which is the solution that is returned by Algorithm 2 at $\gamma \rightarrow \infty$. This means that the difference between u values obtained by Algorithm 2 in quantized and infinite resolution systems increase as number of users increase. Moreover, note that our outcome is in parallel with the finding in [15], which considers quantized systems with no power allocation. Therein the optimal regularization parameter ρ is revealed to be proportional to the user load β at high transmit power regime.

B. Computational Complexity of RZF precoding with Algorithm 2

Computational burden of linear precoding consists of obtaining the precoding matrix once at every coherence time and linear transformation of \mathbf{s} to \mathbf{x} at every transmission. In our case, we obtain the solution for the approximate sum rate maximization in (44) as u^* , \mathbf{w}^* and K^* by Algorithm 2, then we map them to \mathbf{E}_K and \mathbf{P}_K as it is described in Section V-C. Before employing Algorithm 2, we compute all large-scale fading coefficients as $\sigma_m = \frac{\|\mathbf{h}_m\|^2}{N}$ and we compute (c_1, c_2, \dots, c_M) by (42). These operation cost $2MN$ and $3M$ floating point operations (FLOPs), respectively.

The next part that requires FLOPs is the while loop of Algorithm 2. Let us denote the number of iterations that the while loop takes to converge as I . Mercury/waterfilling and bisection search are two main operations that are executed at every iteration to solve (45) and (57), respectively. In the first iteration of the while loop, mercury/waterfilling algorithm is applied with M active users. In most cases, the number of active users does not change after the first iteration so that for $I - 1$ iterations mercury/waterfilling algorithm is applied with $K^{(I)}$ active users, where $K^{(I)}$ is the number of active users that Algorithm 2 obtains as solution. In application of mercury/waterfilling, (47) is solved by employing the bisection search and a look-up table. Here, we neglect the computational complexity of accessing the memory where the look-up tables are stored. Each iteration of bisection search to solve (47) with K users takes $2K$ multiplication and $K - 1$ additions. Hence, an iteration of bisection search to solve (47) with K users costs $\mathcal{O}(3K)$. We empirically observe that equation (47) is satisfied by error of 10^{-6} at approximately $i_{\text{mercury}} \approx 22$ nd

iteration of the bisection search, regardless of value of K . We calculate the total computational complexity of solving (47) in Algorithm 2 as $i_{\text{mercury}}(3M + 3K^{(I)}(I - 1))$ FLOPs.

We solve (57) by finding the regularization parameter u satisfying (58) with bisection search in interval $[0, 1]$. The solution of (58) can be found by the error of 10^{-6} in $i_{\text{bisection}} = 20$ iterations. Each iteration of bisection search consists of computing (59) by using the MMSE look-up tables that we also used to solve (47). For K active users, computation of the numerator and the denominator in (61) costs $2K$ operations each. Computing the fraction in (61) and multiplication by w_m s cost K FLOP each. Multiplication with MMSE values from (60) costs another K operations and $K - 1$ additions more are required to compute (58). As a result, one iteration of bisection search to solve (58) costs approximately $8K$ FLOPs. The total complexity of finding the u satisfying (58) is $i_{\text{bisection}}(8M + (I - 1)K^{(I)})$.

Computing matrix $\mathbf{P}_K = \mathbf{H}_K^H(\mathbf{H}_K\mathbf{H}_K^H + \alpha\mathbf{\Sigma}_K)^{-1}$ is the operation that costs the highest number of FLOPs after completion of the while loop. Computing the term $\mathbf{H}_K\mathbf{H}_K^H$ consists of approximately K^2N operations (taking into account that $\mathbf{H}_K\mathbf{H}_K^H$ is a Hermitian matrix). Computing $(\mathbf{H}_K\mathbf{H}_K^H + \alpha\mathbf{\Sigma}_K)$ hence costs $K^2N + 2K$ FLOPs. If we assume that Cholesky decomposition, forward-substitution and back-substitution is employed to compute the inversion, then the inversion $(\mathbf{H}_K\mathbf{H}_K^H + \alpha\mathbf{\Sigma}_K)^{-1}\mathbf{H}_K$ costs $\frac{K^3}{3} + 2K^2N$ FLOPs. Also, scaling by the entries of $\mathbf{E}_K^{\frac{1}{2}}$ costs KN FLOPs. As a result, the complexity of computing $\mathbf{P}_K\mathbf{E}_K^{\frac{1}{2}}$ is in total $\frac{K^3}{3} + 3K^2N + KN + 2K$ FLOPs. Computing \mathbf{E}_K costs K multiplications and K square root operations.

In most channel realizations, I required for Algorithm 2 to converge is 3. Thus, as number of active users K and N grow large, most of computational complexity is caused by the inversion operation and complexity due to computing the regularization parameter and the power factors becomes negligible. The complexity when $K \rightarrow \infty, M \rightarrow \infty$ and $N \rightarrow \infty$ is $\mathcal{O}(K^3 + K^2N)$.

VII. EXTENSION OF Q-GPI-SEM TO CE QUANTIZATION

In [18], performance of Algorithm 2 in 1-bit MIMO downlink is compared to the state-of-the-art Q-GPI-SEM from [16]. Q-GPI-SEM cannot be applied directly in CE MIMO downlink with higher resolution, since it relies on the additive quantization noise model (AQNM) which is valid if the real and imaginary parts of the precoded signal are quantized separately. A nontrivial extension of Q-GPI-SEM is required. To this aim, we utilize the linear covariance approximation (LCA) model which has been first presented in [28] and enabled for use of CE quantization in [29, Chapter 3].

With few modifications, Fig. 1 can be used to represent the system model with Q-GPI-SEM as well. Unlike Fig. 1, Q-GPI-SEM precoding is done as $\mathbf{x} = \mathbf{P}\mathbf{s}$ such that the power allocation is not carried out via matrix \mathbf{E} but it is included in precoding matrix \mathbf{P} . Also, a transmit power constraint is imposed on the precoded signal such that $\text{tr}(\mathbf{P}\mathbf{P}^H) = \gamma$ and the input \mathbf{s} is assumed to be Gaussian. The steps after precoding remain the same as Fig. 1. Given these changes,

let us first consider the following quantization

$$\mathcal{Q}_{\text{LCA}}(x_n) = r_n \exp(j(\lfloor \frac{\angle x_n}{2\psi} \rceil - \psi)), \forall n, \quad (70)$$

where r_n is the envelope of the quantized output and $\psi = \frac{\pi}{Q}$. On the contrary to (4), each element of \mathbf{x} is quantized with a different envelope r_n . In such quantization operation, one has a freedom to select r_n as the value minimizing $E[|\mathcal{Q}_{\text{LCA}}(x_n) - x_n|^2]$. In case of $x_n \sim \mathcal{CN}(0, \sigma_{x_n}^2)$, the r_n value minimizing $E[|\mathcal{Q}_{\text{LCA}}(x_n) - x_n|^2]$ is given as $r_n = \xi_Q \sigma_{x_n}$ [29]. As a result, when quantization in (70) is applied to all elements of \mathbf{x} with corresponding minimizing r_n , the output can be decomposed by LCA as follows [29]

$$\mathcal{Q}_{\text{LCA}}(\mathbf{x}) = \xi_Q^2 \mathbf{x} + \mathbf{d}_{\text{LCA}}, \quad (71)$$

where \mathbf{x} and \mathbf{d}_{LCA} are uncorrelated. The covariance of distortion \mathbf{d}_{LCA} is given as [29]

$$\mathbf{C}_{\mathbf{d}_{\text{LCA}}\mathbf{d}_{\text{LCA}}} \approx \xi_Q^2 (1 - \xi_Q^2) \text{diag}(\mathbf{P}\mathbf{P}^H). \quad (72)$$

We can reformulate (4) in terms of $\mathcal{Q}_{\text{LCA}}(\cdot)$ such that

$$\mathcal{Q}(\mathbf{x}) = \frac{1}{\xi_Q} \text{diag}(\mathbf{P}\mathbf{P}^H)^{-\frac{1}{2}} \mathcal{Q}_{\text{LCA}}(\mathbf{x}). \quad (73)$$

At this step, we again resort to the asymptotic approximation which revealed in (24) that for RZF precoder $\text{diag}(\mathbf{C}_{\mathbf{xx}})$ converges to a scaled identity matrix. We also here expect that for a reasonable choice of \mathbf{P} , $\text{diag}(\mathbf{P}\mathbf{P}^H)$ asymptotically converges to a scaled identity matrix. Due to the constraint $\text{tr}(\mathbf{P}\mathbf{P}^H) = \gamma$, we approximate $\text{diag}(\mathbf{P}\mathbf{P}^H)$ as $\frac{\gamma}{N} \mathbf{I}_N$. By employing (73) and (71), we can approximate the received signal at the m th user

$$y_m \approx \xi_Q \mathbf{h}_m^H \mathbf{P} \mathbf{s}_m + \xi_Q \sum_{j \neq m} \mathbf{h}_m^H \mathbf{P}_j \mathbf{s}_j + \frac{1}{\xi_Q} \mathbf{h}_m^H \mathbf{d}_{\text{LCA}} + \eta_m. \quad (74)$$

The received quantization distortion power is approximated as

$$\frac{1}{\xi_Q^2} \mathbf{h}_m^H \mathbf{C}_{\mathbf{d}_{\text{LCA}}\mathbf{d}_{\text{LCA}}} \mathbf{h}_m = (1 - \xi_Q^2) \sum_{j=1}^M \mathbf{p}_j^H \text{diag}(\mathbf{h}_m \mathbf{h}_m^H) \mathbf{p}_j, \quad (75)$$

by employing (72) and some algebraic manipulations. As we assume Gaussian inputs, (74) and (75) can be combined to approximate the rate of the m th user as

$$R_m \approx \log_2 \left(\frac{\bar{\mathbf{p}}^H \mathbf{C}_m \bar{\mathbf{p}}}{\bar{\mathbf{p}}^H \mathbf{D}_m \bar{\mathbf{p}}} \right), \quad (76)$$

where

$$\begin{aligned} \mathbf{C}_m &= \text{blkdiag}(\mathbf{G}_m, \mathbf{G}_m \dots \mathbf{G}_m) + \frac{1}{\gamma} \mathbf{I}_{MN}, \\ \mathbf{G}_m &= \xi_Q^2 \mathbf{h}_m \mathbf{h}_m^H + (1 - \xi_Q^2) \text{diag}(\mathbf{h}_m \mathbf{h}_m^H), \\ \mathbf{D}_m &= \mathbf{C}_m - \text{blkdiag}(\mathbf{0}_N, \dots, \xi_Q^2 \mathbf{h}_m \mathbf{h}_m^H, \dots \mathbf{0}_N) \end{aligned} \quad (77)$$

and $\bar{\mathbf{p}}$ is the unit norm vector that is obtained by stacking and normalizing \mathbf{P} , i.e., $\bar{\mathbf{p}} = \frac{\text{vec}(\mathbf{P})}{\sqrt{\gamma}}$. In [16], Q-GPI-SEM is offered as an algorithm that obtains the unit norm solution to the rate maximization problem where rate expressions are in form of (76). We can apply Q-GPI-SEM from [16] with $\mathbf{C}_m, \mathbf{D}_m$ in (77) for Q -level CE quantization (see Section V in [16] for the details). The unit norm stacked vector obtained by Q-GPI-SEM is scaled by $\sqrt{\gamma}$ and reshaped as separate columns in $\mathbf{P} \in \mathbb{C}^{N \times M}$ obeying $\text{tr}(\mathbf{P}\mathbf{P}^H) = \gamma$.

Q-GPI-SEM performs power iterations, where the operation with highest computational cost is inversion of a $N \times N$ matrix. At each power iteration, matrix inversion is performed M

times so that one power iteration's computational complexity is $\mathcal{O}(MN^3)$. For that reason, when the number of active users $K \ll N$, Algorithm 2 has significantly lower computational complexity than Q-GPI-SEM. Furthermore, linear transformation of \mathbf{s} to \mathbf{x} costs $2MN$ FLOPs in Q-GPI-SEM, whereas the precoding is done by $\mathbf{x} = \mathbf{P}_k \mathbf{E}_K \mathbf{s}_K$ in Algorithm 2, which costs $2KN$ FLOPs. If not all users are active, i.e., $K < M$, then we save computational complexity with algorithm 2, which gets larger if the bandwidth is increased.

VIII. NUMERICAL RESULTS

In this section, we provide numerical results for the proposed RZF precoding techniques. We select empirical generalized mutual information (GMI) as the performance metric illustrating the user rates (for the details on how to compute empirical GMI the reader is referred to [30]). Average rate over all M users within the cell is plotted versus transmit SNR γ_{dB} . Curves for the average rates are obtained by averaging over 1000 realizations of the Rayleigh fading channel model. At each channel realization, the large-scale fading coefficient of the m th user is determined from the path loss (PL) as $\sigma_m = \frac{1}{\text{PL}_m}$ and the PL of the m th user is generated as

$$\text{PL}_m \text{ (in dB)} = a + 10b \log_{10}(z_m) + \zeta, \quad (78)$$

where z_m and $\zeta \sim \mathcal{N}(0, \sigma_\zeta^2)$ are the distance from the transmitter and the shadowing factor of the m th user, respectively. Parameters a, b, σ_ζ^2 are given as 61.4, 3.4, 9.7, respectively, which correspond to the non-line-of-sight (NLOS) channel measurements at 28 GHz [31]. The single-antenna users are distributed in a ring-like area with inner radius of 35 m and outer radius of 200 m with uniform probability. Finally, we assume equiprobable distribution for the scenarios with finite input constellations.

A. Comparison of Algorithm 1 and Algorithm 2

In Fig. 2, we see the average rates with RZF precoding obtained by Algorithm 1 and Algorithm 2 in CE MIMO downlink with $N = 64$ antennas. Solid and dashed curves depict the average rates achieved by Algorithm 1 in systems with $M = 8$ and $M = 32$ users, respectively. Colors of the curves are selected according to the combination input constellation and number of CE quantization levels Q . The diamond marks are obtained by applying Algorithm 2 under the same settings as the solid or dashed curves they overlap with. The performance gap between Algorithm 1 and Algorithm 2 is negligible in all depicted settings and we empirically confirm that Algorithm 1 has significantly higher computational complexity². For that reason, quantization-aware RZF (QA-RZF) curves are generated with Algorithm 2 for the rest of the numerical results.

B. Benefits of Quantization Awareness

In this subsection, our proposed QA-RZF precoding is essentially compared to the quantization-ignorant RZF (QI-RZF) and a benchmark with no quantization. To obtain the QI-RZF curve, Algorithm 2 is run with the assumption of

²For example, in CE MIMO downlink with $M = 8, N = 64, Q = 4$ and QPSK inputs, Algorithm 1 takes on the average 8 times to converge in comparison to Algorithm 2.

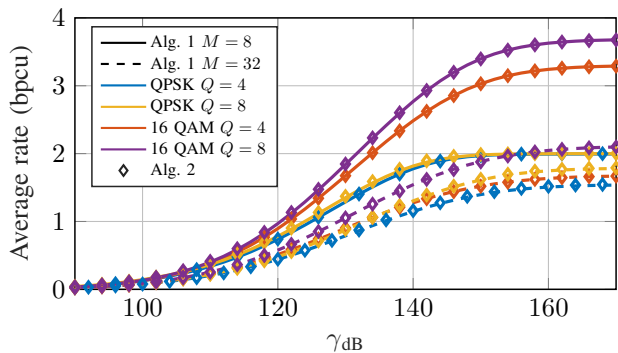


Fig. 2. Average rates of users in CE quantized MIMO downlink with $N = 64$. $M = 8$ for solid curves, $M = 32$ for dashed curves. Different colors represent different input signal constellation and quantization. The diamond marks are obtained by Algorithm 2.

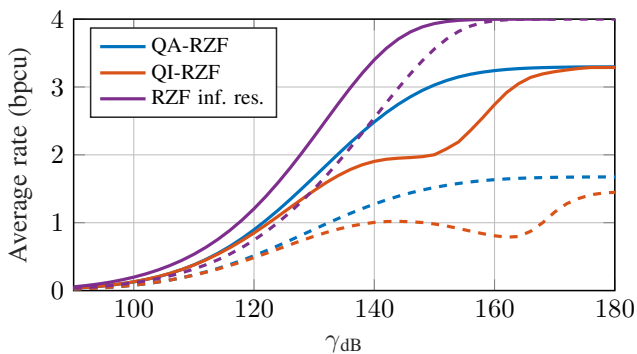


Fig. 3. Average rates of users in MIMO downlink $N = 64$, 16 QAM inputs and $Q = 4$. $M = 8$ for solid curves, $M = 32$ for dashed curves.

no quantization -which can be done by setting $\xi_Q = 1$ when computing c_k values in (42)- and then the precoded signal goes through Q level CE quantization. The benchmark 'RZF inf. res.' is obtained by scaling the precoded signal of QI-RZF to have power of γ and then transmitting it with no quantization. Note that for QI-RZF, the approximate channel gains in (43b) grow very large at $\gamma \rightarrow \infty$. This leads users to almost achieve the natural rate limit, i.e., the maximum rate due to having finite constellation, even with small values of \mathbf{w} , for which $\sum_{k=1}^K w_k < K$. As a result, obtaining the exact solution of (46) requires an idealistic MMSE look-up table with infinite range. In such cases, the mercury/waterfilling implementation does not converge to satisfy (46) and we manually set its solution to $\mathbf{w} = \mathbf{1}_M$. Otherwise, QI-RZF performs even worse at $\gamma \rightarrow \infty$ in CE systems.

Fig. 3 illustrates average rates of users in CE MIMO downlink with 16 QAM inputs, $N = 64$ and $Q = 4$. Solid curves depict the average rates for the system with $M = 8$ users and dashed curves are for $M = 32$. The benefit of taking quantization into account is clearly observed when QA-RZF is compared to QI-RZF. For $M = 8$ and $M = 32$, there are gaps of approximately 5 dB and 6.8 dB around 1.8 and 1 bpcu, respectively. QI-RZF curve diverges from QA-RZF curve as transmit power increases.

On the right side of Fig. 3, we see that the gap between QA-RZF and QI-RZF enlarges when M is increased to 32

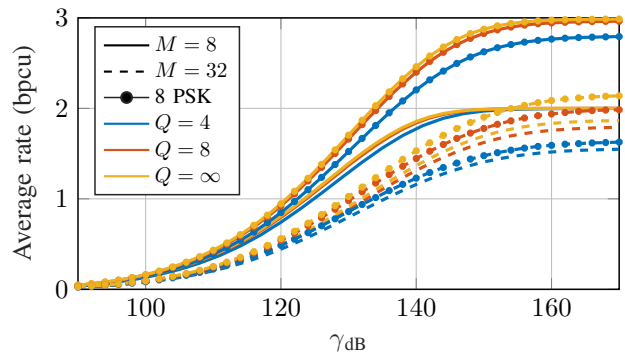


Fig. 4. Average rates of users in CE quantized MIMO downlink with $N = 64$. $M = 8$ for solid curves, $M = 32$ for dashed curves. Different colors represent different input quantization levels. The curves with circle marks are for 8 PSK inputs.

from 8, which can be interpreted via the high transmit power analysis. Both QI-RZF and QA-RZF set $\mathbf{w} = \mathbf{1}_M$ at $\gamma \rightarrow \infty$ so that the gap is not due to the power allocation. On the other hand, from the discussion in Section VI-A we know that the difference between u values obtained for quantized and unquantized systems increases with number of users, which causes the gap between QA-RZF and QI-RZF to enlarge.

Also, we observe that rates achieved by QI-RZF do not consistently increase with the transmit power in Fig. 3. This is caused by the power allocation in QI-RZF at a particular region of high transmit power regime, where the mercury/waterfilling algorithm converges and $\mathbf{w} = \mathbf{1}_M$ is not yet set manually. As the approximate channel gains in (43b) grow large in QI-RZF, the mercury/waterfilling converges to the power allocation that is inversely proportional to the channel gains [25]. This power allocation is clearly far from the optimal uniform-like power allocation of QA-RZF at high transmit power and causes the observed inconsistency.

C. Performances with Different CE Quantization and Modulation Levels

Fig. 4 depicts how QA-RZF performs with various quantization levels and input constellations. The legend has a similar structure as the legend of Fig. 2 with a difference that here colors represent only the quantization levels and curves with circle marks are for 8 PSK inputs. Setting $Q = \infty$ corresponds to infinite resolution phase quantization with unit magnitude. In Fig. 4 shift in Q from 4 to 8 improves rates substantially, whereas increasing Q above 8 is not as effective especially at low user load or low/moderate transmit power. By comparing the cases with QPSK and 8 PSK inputs, we can see that increasing Q makes a bigger difference in higher order modulation.

Fig 5 illustrates rates achieved by QA-RZF in the system with $M = 8$, $N = 64$ and $Q = 4$. Different curves stand for the systems with different input signal constellations. In Fig 5, the combination of two factors determines the performance of QA-RZF. The first factor is the positive effect of higher modulation order such that power allocation is more efficient compared to the low order modulated systems, since stronger users are away from the natural rate limit for a broader range of

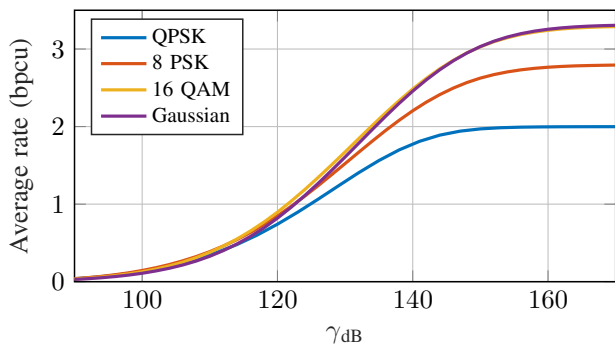


Fig. 5. Average rates of users in MIMO downlink $M = 8$, $N = 64$ and $Q = 4$

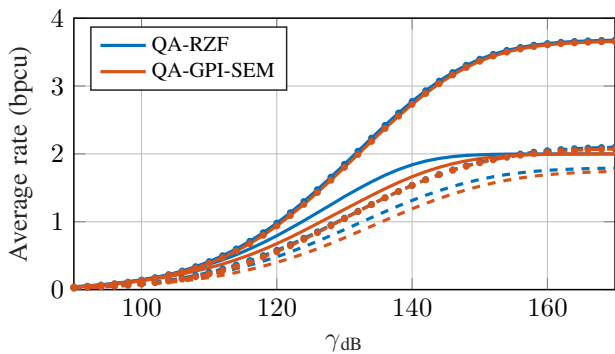


Fig. 6. Average rates of users in the MIMO downlink with QA-RZF and Q-GPI-SEM precoding, $N = 64$ and $Q = 8$. $M = 8$ for solid curves, $M = 32$ for dashed curves. Curves with no markers are for QPSK inputs, curves with circle markers are for 16 QAM.

transmit power. For that reason, there is a tendency to achieve higher rates with higher order modulation. On the other hand, QA-RZF is based on an approximation obtained via (11). As modulation order increases (11) gets more inaccurate at low transmit power. This is why 16 QAM curve is outperformed by 8 PSK curve and curve for Gaussian inputs is outperformed by 8 PSK and 16 QAM curves at low transmit power.

D. Comparison to the State-of-the-Art

Fig. 6 exhibits performance of QA-RZF in comparison to the state-of-the-art method Q-GPI-SEM originally from [16], extended here in Section VII. Number of quantization levels is selected as $Q = 8$. QA-RZF outperforms Q-GPI-SEM especially in systems with QPSK inputs. In systems with 16 QAM inputs, performances of QA-RZF and Q-GPI-SEM are very close. The comparison for Gaussian input has been shown in [18], where again QA-RZF and Q-GPI-SEM curves almost overlap. Also note that results with $Q = 4$ are essentially the same as Fig. 6 and it is depicted in [18] as well. QA-RZF outperforms Q-GPI-SEM in the systems with lower order modulation, since it can be easily adapted for every input constellation, whereas Q-GPI-SEM is designed for Gaussian inputs. Finally, even though QA-RZF cannot outperform Q-GPI-SEM in higher order modulation, it has significantly less computational complexity as it is shown in Section VI-B.

IX. CONCLUSION AND OUTLOOK

In this paper, we presented two algorithms (based on the branch and bound method and alternating optimization) for sum rate maximization in the CE MIMO with RZF precoding. Although alternating optimization obtains a local maximum for the approximate sum rate, it effectively achieves the same sum rate as the branch-and-bound method, which obtains the global maximum for the approximate sum rate. This makes us select the alternating optimization as the main proposed algorithm, since it has a lower computational complexity. To compare our algorithm to the state-of-the-art, we extended the Q-GPI-SEM algorithm to the CE MIMO with higher resolution. The advantages of the proposed method over Q-GPI-SEM is its compatibility with any input signal distribution and significantly lower computational complexity. In future studies, the proposed method can provide a refined initial point for symbol-wise precoding techniques to account for the power allocation. Similarly, it can be used to improve the power allocation for hybrid precoding in CE MIMO downlink significantly.

APPENDIX A

UPPER BOUND TO $R(\mathcal{S})$

Let us rewrite (50) as

$$R(\mathcal{S}) = \max_{\mathbf{w} \geq 0} \sum_{k=1}^{K_S} I(\lambda_k(u_S, K_S) w_k) \text{ s.t. } \sum_{k=1}^{K_S} w_k = K_S, \quad (79)$$

where we denote the optimal (u, K) for (50) as (u_S, K_S) and $\mathbf{w}^*(u_S, K_S)$ is the corresponding optimal power allocation obtained by (46). We define an upper bound $U(\mathcal{S})$ by using the following intermediate bounds

$$\hat{R}(\mathcal{S}) = \max_{\mathbf{w} \geq 0} \sum_{k=1}^{K_S} I(\Lambda_k w_k) \text{ s.t. } \sum_{k=1}^{K_S} w_k = K_S, \quad (80)$$

$$\hat{U}(\mathcal{S}) = \max_{\mathbf{w} \geq 0} \sum_{k=1}^{K_S} I(\Lambda_k w_k) \text{ s.t. } \sum_{k=1}^{K_S} w_k = K_U, \quad (81)$$

$$U(\mathcal{S}) = \max_{\mathbf{w} \geq 0} \sum_{k=1}^{K_U} I(\Lambda_k w_k) \text{ s.t. } \sum_{k=1}^{K_U} w_k = K_U, \quad (82)$$

where we denote $\Lambda_k(u_L, u_U, K_L)$ as Λ_k and it holds that $U(\mathcal{S}) \geq \hat{U}(\mathcal{S}) \geq \hat{R}(\mathcal{S}) \geq R(\mathcal{S})$. Note that we denote Inequality $\hat{R}(\mathcal{S}) \geq R(\mathcal{S})$ is concluded by observing that (80) is a power allocation problem with same transmit power constraint as (79), but with stronger channels due to (53). Inequality $\hat{U}(\mathcal{S}) \geq \hat{R}(\mathcal{S})$ holds, since (81) is a power allocation problem for the same channels as (80) but with a higher power constraint. Finally, one can take the optimal power allocation vector of (81) and pad $K_U - K_S$ zeros to make it a feasible power allocation vector for (82). The rate achieved with this feasible vector in (82) is equal to the optimal rate in (81) so that we conclude $U(\mathcal{S}) \geq \hat{U}(\mathcal{S})$.

APPENDIX B

ENTRIES OF $\mathbf{w}_{U(\mathcal{S})}$ AND THE GLOBAL MAXIMUM

Theorem 4. For a given subset \mathcal{S} , if the optimal power allocation vector for (82), denoted as $\mathbf{w}_{U(\mathcal{S})}$, has less nonzero entries than K_L , then \mathcal{S} does not contain the solution of (49). We arrive to Theorem 4 by combining Lemmas 3 and 4.

Lemma 2. Within a given subset \mathcal{S} , number of nonzero elements in the optimal power allocation vector $\mathbf{w}^*(u_{\mathcal{S}}, K_{\mathcal{S}})$ is upper bounded by the number of nonzero elements in $\mathbf{w}_{\mathcal{U}}(\mathcal{S})$.

Proof. Let us denote number of nonzero entries in optimal \mathbf{w} vectors as $J, \hat{J}, \hat{J}_{\mathcal{U}}, J_{\mathcal{U}}$ for (79), (80), (81) and (82), respectively. From the argumentation in Appendix A, it is clear that $J \leq \hat{J} \leq \hat{J}_{\mathcal{U}}$. In order to compare $\hat{J}_{\mathcal{U}}$ to $J_{\mathcal{U}}$, let us consider the optimality conditions for (81) and (82) respectively as follows

$$\sum_{k=1}^{\hat{J}_{\mathcal{U}}} \frac{1}{\Lambda_k(u_{\mathcal{L}}, u_{\mathcal{U}}, K_{\mathcal{L}})} \text{MMSE}^{-1}\left(\frac{\hat{\mu}_{\mathcal{U}}}{\Lambda_k(u_{\mathcal{L}}, u_{\mathcal{U}}, K_{\mathcal{L}})}\right) = K_{\mathcal{U}}, \quad (83)$$

$$\sum_{k=1}^{J_{\mathcal{U}}} \frac{1}{\Lambda_k(u_{\mathcal{L}}, u_{\mathcal{U}}, K_{\mathcal{L}})} \text{MMSE}^{-1}\left(\frac{\mu_{\mathcal{U}}}{\Lambda_k(u_{\mathcal{L}}, u_{\mathcal{U}}, K_{\mathcal{L}})}\right) = K_{\mathcal{U}}. \quad (84)$$

Terms $\hat{\mu}_{\mathcal{U}}$ and $\mu_{\mathcal{U}}$ are the optimal waterlevels for (81) and (82). Before proceeding recall that $\Lambda_1(u_{\mathcal{L}}, u_{\mathcal{U}}, K_{\mathcal{L}}) \geq \Lambda_2(u_{\mathcal{L}}, u_{\mathcal{U}}, K_{\mathcal{L}}) \dots \geq \Lambda_{K_{\mathcal{L}}}(u_{\mathcal{L}}, u_{\mathcal{U}}, K_{\mathcal{L}})$. Now let us assume that $J_{\mathcal{U}} < \hat{J}_{\mathcal{U}}$. In this case, (83) and (84) can only hold if $\mu_{\mathcal{U}} < \hat{\mu}_{\mathcal{U}}$. On the other hand, if the optimal power allocation vector in (82) has $J_{\mathcal{U}}$ nonzero entries, then it holds that $\Lambda_{\hat{J}_{\mathcal{U}}}(u_{\mathcal{L}}, u_{\mathcal{U}}, K_{\mathcal{L}}) \leq \mu_{\mathcal{U}} < \Lambda_{J_{\mathcal{U}}}(u_{\mathcal{L}}, u_{\mathcal{U}}, K_{\mathcal{L}})$. Similarly, if the optimal power allocation vector in (80) has $\hat{J}_{\mathcal{U}}$ nonzero entries, then $\hat{\mu}_{\mathcal{U}} < \Lambda_{\hat{J}_{\mathcal{U}}}(u_{\mathcal{L}}, u_{\mathcal{U}}, K_{\mathcal{L}})$. As a result, it must also hold that $\hat{\mu}_{\mathcal{U}} < \mu_{\mathcal{U}}$, which leads to a contradiction such that $J_{\mathcal{U}} < \hat{J}_{\mathcal{U}}$ cannot hold. We conclude that $J \leq \hat{J} \leq \hat{J}_{\mathcal{U}} \leq J_{\mathcal{U}}$. \square

Lemma 3. For a subset $\mathcal{S} = \{(u, K) | u \in (u_{\mathcal{L}}, u_{\mathcal{U}}), K \in \{K_{\mathcal{L}}, \dots, K_{\mathcal{U}}\}\}$, if sum rate maximizing power allocation vector $\mathbf{w}^*(u_{\mathcal{S}}, K_{\mathcal{S}})$ has less nonzero elements than $K_{\mathcal{L}}$, then \mathcal{S} does not contain the solution of (49).

Proof. Let us assume that $\mathbf{w}^*(u_{\mathcal{S}}, K_{\mathcal{S}})$ has $J < K_{\mathcal{L}}$ nonzero elements, which means that last $K_{\mathcal{S}} - J$ entries of $\mathbf{w}^*(u_{\mathcal{S}}, K_{\mathcal{S}})$ are equal to 0. For subset \mathcal{S} , the optimal SNR values of users reads as

$$\text{SNR}_k = \frac{\frac{N}{K_{\mathcal{S}}} - u_{\mathcal{S}}^2}{\frac{K_{\mathcal{S}}-1}{K_{\mathcal{S}}}(1-u_{\mathcal{S}})^2 + c_k} w_k^*(u_{\mathcal{S}}, K_{\mathcal{S}}) \quad (85)$$

for $k = 1, 2, \dots, J$. For $k = J+1, \dots, K_{\mathcal{S}}$, $\text{SNR}_k = 0$. Note that $\sum_{k=1}^{K_{\mathcal{S}}} w_k^*(u_{\mathcal{S}}, K_{\mathcal{S}}) = K_{\mathcal{S}}$. Let us consider an alternative system with $u = u_{\mathcal{S}}$ and $K = J$, which is not in the subset \mathcal{S} . For such system, setting $\bar{w}_k = \frac{J}{K_{\mathcal{S}}} w_k^*(u_{\mathcal{S}}, K_{\mathcal{S}})$ for $k = 1, \dots, J$, is a valid power allocation as it satisfies $\sum_{k=1}^J \bar{w}_k = J$. As a result, the SNRs values in system with $u_{\mathcal{S}}, J$ and $\bar{\mathbf{w}}$ reads as

$$\bar{\text{SNR}}_k = \frac{\frac{N}{K_{\mathcal{S}}} - \frac{J}{K_{\mathcal{S}}} u_{\mathcal{S}}^2}{\frac{J-1}{J}(1-u_{\mathcal{S}})^2 + c_k} w_k^*(u_{\mathcal{S}}, K_{\mathcal{S}}) \quad (86)$$

for $k = 1, \dots, J$. It is clear that $\bar{\text{SNR}}_k > \text{SNR}_k$, which implies that the optimal rates achieved by active users in \mathcal{S} are less than the rates achieved in the alternative system with $u = u_{\mathcal{S}}, K = J$ and $\bar{\mathbf{w}}$. As the alternative system is also included in the initial set \mathcal{S}_0 , it is clear that \mathcal{S} does not contain the solution of (49). \square

REFERENCES

[1] F. Rusek, D. Persson, B. K. Lau, E. G. Larsson, T. L. Marzetta, O. Edfors, and F. Tufvesson, "Scaling up mimo: Opportunities and challenges with very large arrays," *IEEE Signal Process. Mag.*, vol. 30, no. 1, pp. 40–60, 2013.

[2] E. G. Larsson, O. Edfors, F. Tufvesson, and T. L. Marzetta, "Massive mimo for next generation wireless systems," *IEEE Commun. Mag.*, vol. 52, no. 2, pp. 186–195, 2014.

[3] L. Lu, G. Y. Li, A. L. Swindlehurst, A. Ashikhmin, and R. Zhang, "An overview of massive mimo: Benefits and challenges," *IEEE J. Sel. Topics Signal Process.*, vol. 8, no. 5, pp. 742–758, 2014.

[4] O. Blume, D. Zeller, and U. Barth, "Approaches to energy efficient wireless access networks," in *2010 4th International Symposium on Communications, Control and Signal Processing (ISCCSP)*, 2010, pp. 1–5.

[5] F. H. Raab, "Average efficiency of class-g power amplifiers," *IEEE Trans. Consum. Electron.*, vol. CE-32, no. 2, pp. 145–150, 1986.

[6] S. Jacobsson, G. Durisi, M. Coldrey, T. Goldstein, and C. Studer, "Quantized precoding for massive mu-mimo," *IEEE Trans. Commun.*, vol. 65, no. 11, pp. 4670–4684, 2017.

[7] A. S. Nedelcu, F. Steiner, and G. Kramer, "Low-resolution precoding for multi-antenna downlink channels and ofdm," *Entropy*, vol. 24, no. 4, 2022. [Online]. Available: <https://www.mdpi.com/1099-4300/24/4/504>

[8] H. Jedda, A. Mezghani, A. L. Swindlehurst, and J. A. Nossek, "Quantized constant envelope precoding with psk and qam signaling," *IEEE Trans. Wireless Commun.*, vol. 17, no. 12, pp. 8022–8034, 2018.

[9] T. Yoo and A. Goldsmith, "On the optimality of multiantenna broadcast scheduling using zero-forcing beamforming," *IEEE J. Sel. Areas Commun.*, vol. 24, no. 3, pp. 528–541, 2006.

[10] S. Wagner, R. Couillet, M. Debbah, and D. T. M. Slock, "Large system analysis of linear precoding in correlated mimo broadcast channels under limited feedback," *IEEE Trans. Inf. Theory*, vol. 58, no. 7, pp. 4509–4537, 2012.

[11] R. Muharar, R. Zakhour, and J. Evans, "Optimal power allocation and user loading for multiuser mimo channels with regularized channel inversion," *IEEE Trans. Commun.*, vol. 61, no. 12, pp. 5030–5041, 2013.

[12] L. Sanguinetti, E. Björnson, M. Debbah, and A. L. Moustakas, "Optimal linear precoding in multi-user mimo systems: A large system analysis," in *2014 IEEE Global Communications Conference*, 2014, pp. 3922–3927.

[13] A. K. Saxena, I. Fijalkow, and A. L. Swindlehurst, "Analysis of one-bit quantized precoding for the multiuser massive mimo downlink," *IEEE Trans. Signal Process.*, vol. 65, no. 17, pp. 4624–4634, 2017.

[14] A. K. Saxena, A. Mezghani, and R. W. Heath, "Linear ce and 1-bit quantized precoding with optimized dithering," *IEEE Open J. Signal Process.*, vol. 1, pp. 310–325, 2020.

[15] J. Xu, W. Xu, F. Gong, H. Zhang, and X. You, "Optimal multiuser loading in quantized massive mimo under spatially correlated channels," *IEEE Trans. Veh. Technol.*, vol. 68, no. 2, pp. 1459–1471, 2019.

[16] J. Choi, J. Park, and N. Lee, "Energy efficiency maximization precoding for quantized massive mimo systems," *IEEE Trans. Wireless Commun.*, vol. 21, no. 9, pp. 6803–6817, 2022.

[17] F. Askerbeyli, W. Xu, and J. A. Nossek, "Power allocation in 1-bit massive mimo downlink with zero-forcing precoding," in *2023 IEEE 34th Annual International Symposium on Personal, Indoor and Mobile Radio Communications (PIMRC)*, 2023, pp. 1–6.

[18] —, "Sum rate maximization for regularized zero-forcing precoder in 1-bit mimo," in *2023 IEEE 98th Vehicular Technology Conference (VTC2023-Fall)*, 2023, pp. 1–6.

[19] J. J. Busgang and J. J. Busgang, "Crosscorrelation functions of amplitude-distorted gaussian signals," *Tech. Rep. 216, Research Lab. Electron*, 1952.

[20] H. Jedda and J. A. Nossek, "On the statistical properties of constant envelope quantizers," *IEEE Commun. Lett.*, vol. 7, no. 6, pp. 1006–1009, 2018.

[21] J. Evans and D. Tse, "Large system performance of linear multiuser receivers in multipath fading channels," *IEEE Trans. Inf. Theory*, vol. 46, no. 6, pp. 2059–2078, 2000.

[22] A. Papoulis and H. Saunders, "Probability, random variables and stochastic processes (2nd edition)," *Journal of Vibration and Acoustics-transactions of The Asme*, vol. 111, pp. 123–125, 1989. [Online]. Available: <https://api.semanticscholar.org/CorpusID:110934753>

[23] D. Arnold, H.-A. Loeliger, P. Vontobel, A. Kavcic, and W. Zeng, "Simulation-based computation of information rates for channels with memory," *IEEE Trans. Inf. Theory*, vol. 52, no. 8, pp. 3498–3508, 2006.

[24] D. Guo, S. Shamai, and S. Verdú, "Mutual information and minimum mean-square error in gaussian channels," *IEEE Trans. Inf. Theory*, vol. 51, no. 4, pp. 1261–1282, 2005.

[25] A. Lozano, A. Tulino, and S. Verdú, "Mercury/waterfilling: optimum power allocation with arbitrary input constellations," in *Proceedings. International Symposium on Information Theory, 2005. ISIT 2005.*, 2005, pp. 1773–1777.

- [26] B. Matthiesen, C. Hellings, E. A. Jorswieck, and W. Utschick, "Mixed monotonic programming for fast global optimization," *IEEE Trans. Signal Process.*, vol. 68, pp. 2529–2544, 2020.
- [27] H. Tuy, T. Hoang, T. Hoang, V.-n. Mathématicien, T. Hoang, and V. Mathematician, *Convex analysis and global optimization*. Springer, 1998.
- [28] A. Mezghani, R. Ghiat, and J. A. Nossek, "Transmit processing with low resolution d/a-converters," in *2009 16th IEEE International Conference on Electronics, Circuits and Systems - (ICECS 2009)*, 2009, pp. 683–686.
- [29] H. Jedda, "Quantized constant envelope transmit signal processing," Dissertation, Technische Universität München, München, 2018.
- [30] A. Nedelcu, F. Steiner, M. Staudacher, G. Kramer, W. Zirwas, R. S. Ganesan, P. Baracca, and S. Wesemann, "Quantized precoding for multi-antenna downlink channels with magiq," in *WSA 2018; 22nd International ITG Workshop on Smart Antennas*, 2018, pp. 1–8.
- [31] M. K. Samimi and T. S. Rappaport, "3-d millimeter-wave statistical channel model for 5g wireless system design," *IEEE Trans. Microw. Theory Tech.*, vol. 64, no. 7, pp. 2207–2225, 2016.